OPTICAL PERFORMANCE OF SOLAR POWER TOWERS WITH CONICAL SECONDARY CONCENTRATORS

Perry Ni

A THESIS SUBMITTED TO

THE FACULTY OF GRADUATE STUDIES

IN PARTIAL FULFILLMENT OF THE REQUIREMENTS

FOR THE DEGREE OF

MASTER OF APPLIED SCIENCE

GRADUATE PROGRAM IN MECHANICAL ENGINEERING

YORK UNIVERSITY

TORONTO, ONTARIO

April 2022

Abstract

Solar power towers are a type of concentrating solar power system that enable temperatures of over 1500° C, allowing high efficiency electrical conversion and the creation of solar fuels which can replace CO_2 emitting resources such as oil. Efficient operation of solar towers is achieved through solar concentration in the form of heliostats and conical secondary concentrators. A multi-focus field is proposed allowing for a single tower to have three separate cavity receivers each with its own accompanying polar field of heliostats. Multi-focus fields proved to have comparable power and efficiency levels to single tower north facing fields and were more resilient to slope error. Conical secondary concentrators are a viable alternative to compound parabolic concentrators and have more variability in both concentration ratio as well as acceptance angle. A design map is presented to allow for cones to match either the optical efficiency or concentration ratio of CPCs.

Acknowledgements

I would like to express my gratitude to my supervisor, Dr. Thomas A. Cooper, for accepting me into the CooperLab research group and providing me with constant encouragement and guidance throughout my Masters studies. I am also thankful to Dr. Paul G. O'Brien for his advice and feedback on my project.

I acknowledge the support of the Natural Sciences and Engineering Research Council of Canada (NSERC). I would also like to gratefully acknowledge the company of Synhelion SA for the funding which enabled this research to be conducted.

Lastly, I would like to thank my parents for their continued support.

Table of Contents

List of Figures

Chapter 1. Introduction

1.1 Motivation

Solar energy is a completely renewable and abundant energy source that provides the earth with 5600 times the yearly energy expenditure [1]. Thus, the ability to collect and harness as much of that solar energy as possible is becoming increasingly important, especially with concerns such as depleting fossil fuels and global warming. Concentrating solar power (CSP) systems are one of the many ways that are being researched and developed to improve solar energy's conversion efficiency and enable ultra-high temperature applications. CSP towers utilize faceted mirrors called heliostats arranged in a field to reflect irradiation to a centralized and elevated receiver. The solar radiation reflected toward the tower are further concentrated through a secondary concentrator before reaching the receiver. The design of all the aforementioned components affects the optical performance and efficiency of the CSP system and need to be improved and optimized. CSP has a very low CO_2 equivalent of 20 grams per kWh as opposed to the combustion of coal which has a CO_2 equivalent of 1000 g/kWh [2]. Traditional cylindrical solar tower systems will provide concentration in the 600-1000 suns range [3]. However, the goal is to enable ultra-high temperature greater than 1500 °C which requires higher concentration ratios C_g & a cavity type receiver as opposed to cylindrical receivers with a 360° surrounding field. Therefore, the development and improvement in efficiency of two-stage CSP tower systems will both increase its implementation rate as well as decrease the cost of electricity that will be produced.

Regarding the secondary concentrator, compound parabolic concentrators (CPCs) are considered nearly ideal concentrators. However, due to their non developable geometry, CPCs are expensive

to manufacture and cannot be made from a singular die due to varying sizes at different acceptance angles. In contrast, cones and conical approximations have very simple geometry as they span directly from inlet to outlet and can be easier and cheaper to manufacture. For example, a single die of a fixed angle can be used to create cones of any size, given it is smaller than the die itself. This makes conical concentrators a very attractive alternative to CPCs. Thus, there is high motivation to make this cheaper alternative as high performance and efficient as possible. The current literature available also lacks in conical concentrator design methods of arbitrary concentration ratio and length which is exactly what the study presented in this thesis answers.

1.2 Literature Review

The state of the art technology of solar power tower (SPT) projects that use concentrating solar power are outlined by NREL [4]. Currently, 13% of CSP projects are of the SPT design while the rest consist of parabolic troughs, linear Fresnel concentrators as well as parabolic dishes [5]. The known advantages of SPT are that they are capable of achieving solar fluxes of 200 kW/m^2 to 1000 kW/m^2 which allow for high temperature receiver cavities [6]. These solar fluxes are achieved through solar concentration from heliostats, which are mirrors or groups of mirrors, to a single cavity receiver. Heliostat fields attribute to half of the cost of the SPT system as well as more than 40% of overall energy losses [7][8]. Due to their high cost and the room for improvement, heliostat design and configuration is an area of interest. The most commonly accepted configuration is having the SPT face north while the heliostats are placed in front of the tower, facing south as confirmed by Wei et al. [9].

Traditional SPTs with cylindrical receivers provide concentration in the 500-600 suns range [3] while SPTs with cavity receivers and polar fields can achieve temperatures of above 1000 °C [10]. There also exists field configurations that take advantage of both the cylindrical field heliostat setup as well as cavity receiver temperatures which this thesis defines as multi focus. The Khi Solar One based in South Africa that has three cavity receivers [11].

1.3 Research Question

The main research question is how to effectively design CSP tower systems for the specific application of ultra-high temperature cavity receivers. This includes the design of the primary concentration system in the form of heliostat fields, the tower and receiver, as well as the secondary concentrator. To optimize the efficiency and power to receiver of a CSP tower, all components need to be designed in harmony. Typically, CSP towers have one field dedicated to one tower, but the addition of two more side fields would reduce the cost of needing to build two additional towers. The main concern is whether the lower number of heliostats available in each field can be justified by the reduction in towers needed. As for the design of the secondary concentrator, the question is whether and how a conical concentrator can be designed to become a viable replacement for the CPC. The cone can prove to be a viable replacement if it can surpass the CPC in optical efficiency or if it is able to provide sufficient optical efficiency at a lower cost. There is also interest in whether conical concentrators have any unique advantages in optical concentration.

1.4 Objectives

This thesis investigates the design of CSP towers and conical secondary concentrators with the overarching goal of enabling ultra-high temperature cavity receivers through high efficiency solar concentration. The main objectives of this research were to:

1. Primary concentrator: Design and improve primary solar tower concentration systems for cavity receivers through the exploration of multi focus solar towers and heliostat field configurations (Chapter 3)
2. Secondary concentrator: Provide optical design principles to guide the selection of nonimaging conical secondary concentrators that are high in optical efficiency and low cost (Chapter 4)

1.5 Research Approach and Thesis Structure

The general topics are introduced in Chapter 2: Theory and Background and include items such as solar concentration and concentrating solar power towers.

Chapter 3: Concentrating Solar Power Towers focuses on the primary concentrator: the heliostat field and tower design. SolarPILOT was used to design CSP tower configurations. Each component of the CSP field and tower can be adjusted and changed in SolarPILOT to create the geometries and plots as shown in Figure 8. Various configurations and combinations were simulated with the goal of minimizing field size, tower height, receiver size, as well as keeping the heliostat size to a minimum while maintaining the minimum power output of 1MW/receiver.

A single focus north field was created as a baseline for comparison against the proposed multi focus field with three receivers.

In Chapter 4: Conical Secondary Concentrators, we begin by determining the performance of CPCs and conical concentrators sized to match the size of CPCs. Then, directional acceptance plots and transmission-angle curves were created to explore the directional dependence of incoming radiation. Next, the effects of cone length and cone angle were investigated which led to a design map allowing for optical designers to determine the optical efficiency of any combination of length l and C_g. A method to calculate for the optical efficiency when the average number of reflections is known is also verified.

A summary is provided in Chapter 5: Conclusions and Outlook which also provides the future outlook and outlines work that can be done to build upon this thesis.

1.6 Thesis Summary

Solar energy is a renewable and abundant resource that provides the earth with more energy than the world consumes. Concentrating solar power, CSP, technologies produce sustainable and clean, utility scale electricity. As such, developments in CSP in the form of improving optical efficiency of solar power towers and central receiver systems is important. Advanced simulation techniques were utilized to analyze the optics of solar power tower/central receiver systems with cavity receivers. Solar power tower, systems have primary concentration in the form of heliostats to redirect solar irradiation from a field on to a secondary concentrator in front of the receiver on an

elevated tower. This thesis investigates the suitability of solar towers for ultra-high temperature solar cavity receiver applications and develops primary and secondary optical designs tailored to this application. The investigated design parameters included heliostat size, canting, placement, aim method and slope error, tower height, receiver size and acceptance angle and field size and position. SolarPILOT was used as the simulation software for tower and heliostat design while Monte Carlo ray tracing was used in investigating conical secondary concentrators. Results have shown that multi-focus fields are more resilient to slope error while remaining competitive in optical efficiency and power to receiver comparisons.

A detailed analysis of the optical performance of cones and conical approximations to the 3D (revolved) compound parabolic concentrator is presented in this thesis. The performance metrics used include acceptance efficiency, optical efficiency, transmission-angle curves, directional acceptance maps, and average number of reflections which were all investigated via Monte-Carlo ray-tracing methods. Cones have the potential to be cheaper alternatives to compound parabolic concentrators (CPCs) due to their developable surface which make them easier to manufacture. The simplest approach to approximate a CPC by a cone is to construct a cone that spans directly from the inlet to the outlet of the underlying CPC. In this way, the inlet aperture, outlet aperture, and length of the cone are matched to the underlying CPC. We refer to this most basic approximation as a "matched cone approximation". Interestingly, we found that when matching cones to CPCs with acceptance angles in the range 10 to 60°, the resulting cones are nearly self-similar, in that their apex angle is confined to the range 7 to 11°. Notably, cones with a fixed 10° apex angle were found to outperform the matched cones for acceptance angles ranging from 20 to 42°. This is fortuitous, since a single die could be utilized to construct 10° cones of any size and

acceptance angle. When matched to CPCs with acceptance angles in the range of 10 to 60°, the acceptance efficiency of matched cones spanned 71% to 97%, compared to the 96% to 99% achieved by the CPCs. However, the difference in performance between cones and CPCs decreases as acceptance angle is increased. The relative performance of the matched cone is poorer at smaller acceptance angles but is small at larger acceptance angles. In theory, acceptance efficiency can be improved by increasing cone length. For infinitely long cones, ray rejection vanishes, and cones of all acceptance angles approach 100% acceptance in the infinite-length limit. Although lengthening cones improve acceptance efficiency, the increased length results in a higher number of average reflections which causes lower optical efficiency when the surface of the reflector has a realistic reflectance value, anything lower than 1. An approach for calculating the average number of reflections as well as predicting the optical performance of known geometries using the average number of reflections is verified. A design map showcasing the effects of varying geometric concentration and cone concentrator length is presented. This design map can be used to determine the optical efficiency of any relevant combination of cone length and concentration ratio, inlet/outlet aperture ratio. Overall, the unique advantages in optical performance of cones and lower manufacturing cost make cones and conical approximations attractive substitutions to the CPC.

Chapter 2. Theory and Background

2.1 Solar Concentration

Solar concentration is the process of focusing solar radiation to achieve higher light intensity, thus enabling higher temperatures and more efficient energy conversion. There are two main classes of solar concentration: line focus and point focus. Figure 1 shows that within the two main classes, there are four main designs: parabolic troughs, linear Fresnel reflectors, parabolic dishes, and concentrating towers [12]. CSP has the ability to achieve high temperatures which is advantageous in energy conversion as seen in the Carnot efficiency equation:

$$\eta = 1 - \frac{T_{\text{cold}}}{T_{\text{hot}}} \qquad (1.1)$$

For the creation of solar fuels, Steinfeld et al. [13] notes that for typical mean flux concentrations ratios between 1000 and 12,000 suns, the ideal cavity temperature ranges between 800 to 1300 K. For higher solar flux concentration ratios, higher temperatures are required to maximize efficiency. Therefore, increasing concentration ratio and optical efficiency are closely tied to ultra-high cavity temperatures.

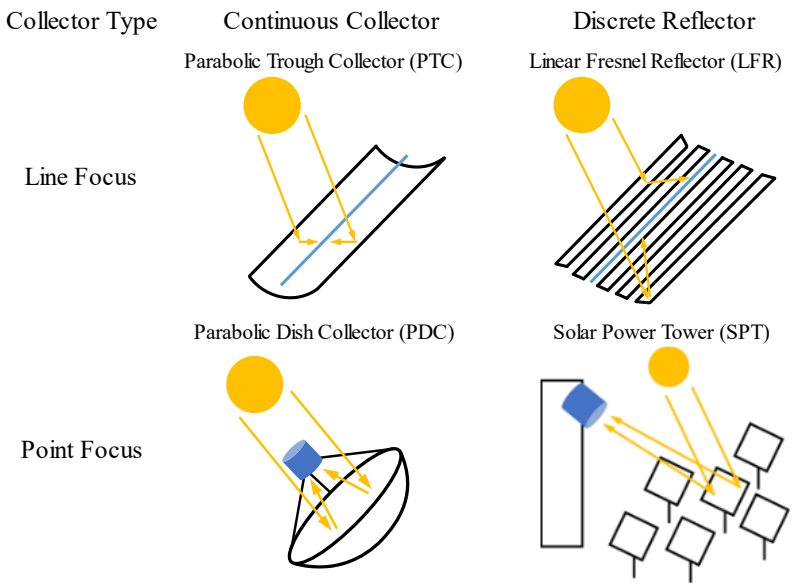

Figure 1. Classification by reflector geometry of the commonly accepted CSP systems. Yellow arrows represent Sun radiation, blue structures symbolize solar receivers, black structures correspond to solar reflectors. Figure adapted from Ref. [12].

2.1.1 Concentrating Solar Power Towers

Concentrating solar power (CSP) towers consist of a heliostat field and a central receiver mounted on a central tower as depicted in Figure 2. CSP towers can either have surrounding fields or polar fields, like the ones outlined in this thesis and seen in Figure 8. Surrounding fields have heliostats surrounding the central tower in every direction and often have cylindrical receivers [12]. Meanwhile, polar fields often utilize cavity receivers, which have the ability to attain temperatures above 1000 °C [10]. Existing CSP tower plants include the Ashalim Plot B (Israel), which has a surrounding field paired with an external receiver, and the PS20 (Spain), which has a polar field paired with a cavity receiver [12].

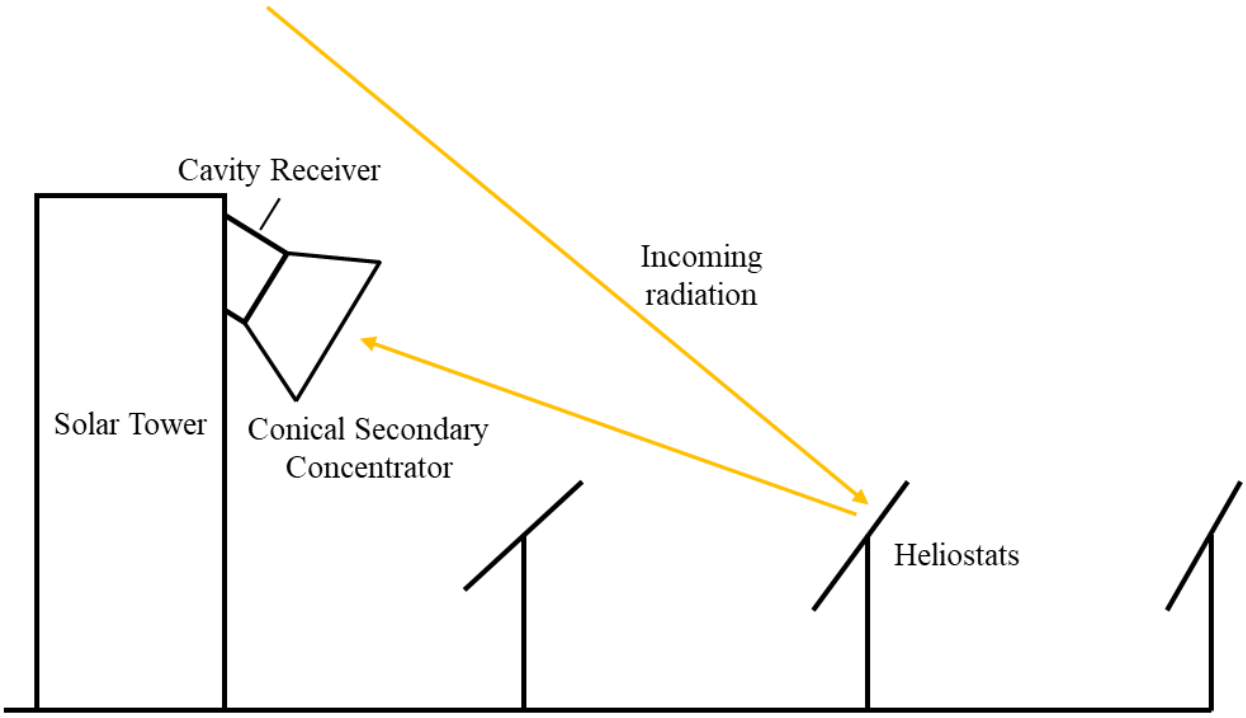

Figure 2. Schematic of solar tower components.

2.2 Concentration Ratio

The geometric concentration ratio C_g is the ratio of the collecting area to the receiver area:

$$C_g = \frac{A_i}{A_o} \tag{1.2}$$

For CSP towers, the C_g is equal to the sum of the surface area of all heliostats over the surface area of the receiver inlet:

$$C_g = \frac{\sum A_{\text{heliostat}}}{A_{\text{receiver}}} \tag{1.3}$$

For secondary concentrators, C_g is the ratio between inlet and outlet apertures as seen in test. For a secondary concentrator with circular inlet and outlet apertures, the equation is the following:

$$C_g = \frac{A_i}{A_o} = \frac{\pi \cdot r_i^2}{\pi \cdot r_o^2} \quad (1.4)$$

Meanwhile, the thermodynamic limit of maximum concentration for full collection of all radiation within a cone angle of θ_i is expressed as the following [14]:

$$C_{g,\max} = \frac{1}{\sin^2 \theta_i} \quad (1.5)$$

where θ_i can have a minimum value of 0.269° (4.7 milliradian) as that is the half angle of solar radiation reaching the earth.

2.2.1 Primary Concentrator

The primary concentrators of CSP towers are the heliostats that reflect radiant power directly from the sun to the receiver mounted on the tower as depicted in Figure 2.

2.2.2 Secondary Concentrator

Secondary concentrators within CSP tower cavity systems are used to further concentrate radiation after it has reached the receiver on the tower. One common secondary concentrator is the revolved compound parabolic concentrator (CPC), which is a three-dimensional, rotationally symmetric, nonimaging optical concentrator which is nearly ideal in that it achieves the theoretical geometric concentration ratio $C_{g,\max} = 1/\sin^2 \theta_i$ [14], [15].

While CPCs are high performing, its intrinsic curvature make it difficult and costly to manufacture. In contrast, cones have very simple geometry due to their developable surface and have the

potential for simpler and less costly manufacturing. Therefore, there is great interest in making cones viable substitutions for the CPC.

2.3 Acceptance Angle

Acceptance angle θ_i is formally defined by Eq. (1.5) and expressed as:

$$\theta_i = \arcsin\left(\frac{1}{\sqrt{C_g}}\right) \tag{1.6}$$

From Eq. (1.6), we see that θ_i is purely a function of C_g and independent of receiver geometry such as l. Coincidentally, the θ_i of CPCs are equal to the slant angle, the line diagonal from the edge of the inlet aperture to the opposite edge of the outlet aperture as seen in Figure 3. For matched cones, the θ_i and slant angle are the same as the CPC of the same θ_i. However, when the l of cones is changed, the θ_i remains the same as long as the inlet and outlet apertures remain the same. The only change is in the slant angle.

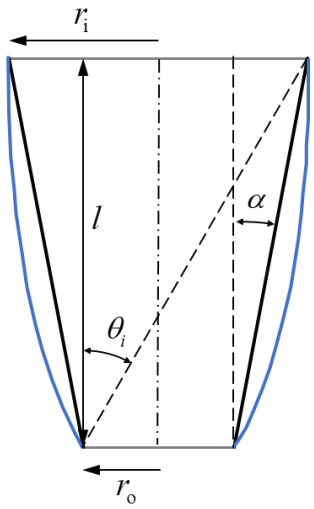

Figure 3. Geometry of a θ_i = 30° CPC and matched cone.

2.4 General Ray-Tracing Procedure

Monte Carlo ray-tracing was the method used in all optical performance evaluations of both CSP primary concentrators using SolTrace, an embedded ray tracing engine within SolarPILOT [16] and secondary concentrators using a code based on VeGaS+, which was developed at ETH Zurich[1] [17]. The program used is a stochastic ray-tracing program that uses a large number of rays to determine propagation of radiant energy through the system. The system starts with an emitting source, which can be specified to be diffuse and have a cone angle θ_i or be collimated. Each surface within the system can either reflect, absorb, or act as a counter surface. The program uses collision-based ray-tracing where all rays have equal power. Efficiency is then determined by the fraction of rays that reach the target. Figure 4 [18] shows the random Monte-Carlo ray-tracing (MCRT) error associated with simulations having N number of rays. Since the number of rays traced per simulation in this thesis range between 10^5 -10^8, the random error is expected to be between 10^{-3} and 10^{-4}.

The error associated with every MCRT simulation is due to its random nature. The magnitude of the error is dependent on the number of rays traced meaning that lower error can be expected as the number of rays traced increases. The relative population standard deviation was presented by Cooper et al. and plotted in Figure 4 [18]:

$$\frac{\sigma}{\langle \eta_{\mathrm{acc}} \rangle} = \frac{\sqrt{\frac{1}{N}\sum_{j=1}^{N} \eta_{\mathrm{acc},j} - \langle \eta_{\mathrm{acc}} \rangle}}{\langle \eta_{\mathrm{acc}} \rangle} \qquad (1.7)$$

[1] The code was developed in the group of Prof. Aldo Steinfeld at ETH Zurich.

where N is the number of simulations run and $\langle \eta_{acc} \rangle$ is the average value of η_{acc}.

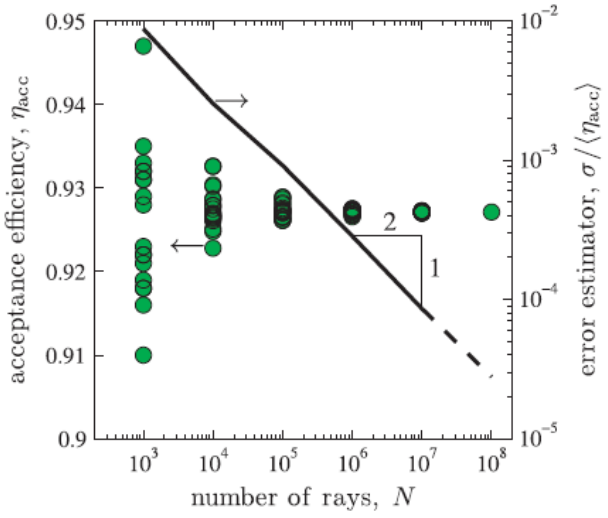

Figure 4. Monte Carlo error in acceptance efficiency of a square CPC with θ_i = 30° for different numbers of rays. The markers show the scatter in the Monte Carlo results of 20 runs for each N performed with different random seeds. The line shows the relative standard deviation of the runs and is a good estimator of the accuracy of the Monte Carlo result. Figure taken from Ref. [18].

Chapter 3. Concentrating Solar Power Towers

3.1 Design Parameters

3.1.1 Tower and Receiver Design

When designing a CSP tower system, the tower and receiver are two key aspects. The height of the tower determines the height at which the receiver is mounted. The height of the receiver consequently affects the positions available to heliostats due to geometry as direct line of sight is required for radiation to be redirected to the receiver. The size, orientation and acceptance angles of the receiver are also considered. All these design parameters can be specified in SolarPILOT, a tool developed by NREL to design and optimize CSP tower plants as seen in Figure 5.

3.1.2 Heliostats

Heliostats are reflectors that redirect and concentrate solar irradiance toward the solar tower. They can be single mirrors or a group of mirrors that span to upwards of 148 m^2 in area [19]. The heliostats described in this thesis consist of square flat mirrors called facets. The use of multiple flat facets to construct a single heliostat enables both canting and lower manufacturing costs. Canting is the aiming method such that each single facet is pointed toward the center of the receiver inlet creating a tighter flux profile and leading to higher optical efficiency as seen in Figure 6 (b). Meanwhile, flat mirrors are cheaper than mirrors with curvature. The design and placement of heliostats depend on many other aspects of CSP tower design such as tower height, field limitations, receiver size and acceptance angle, as well as geographic location.

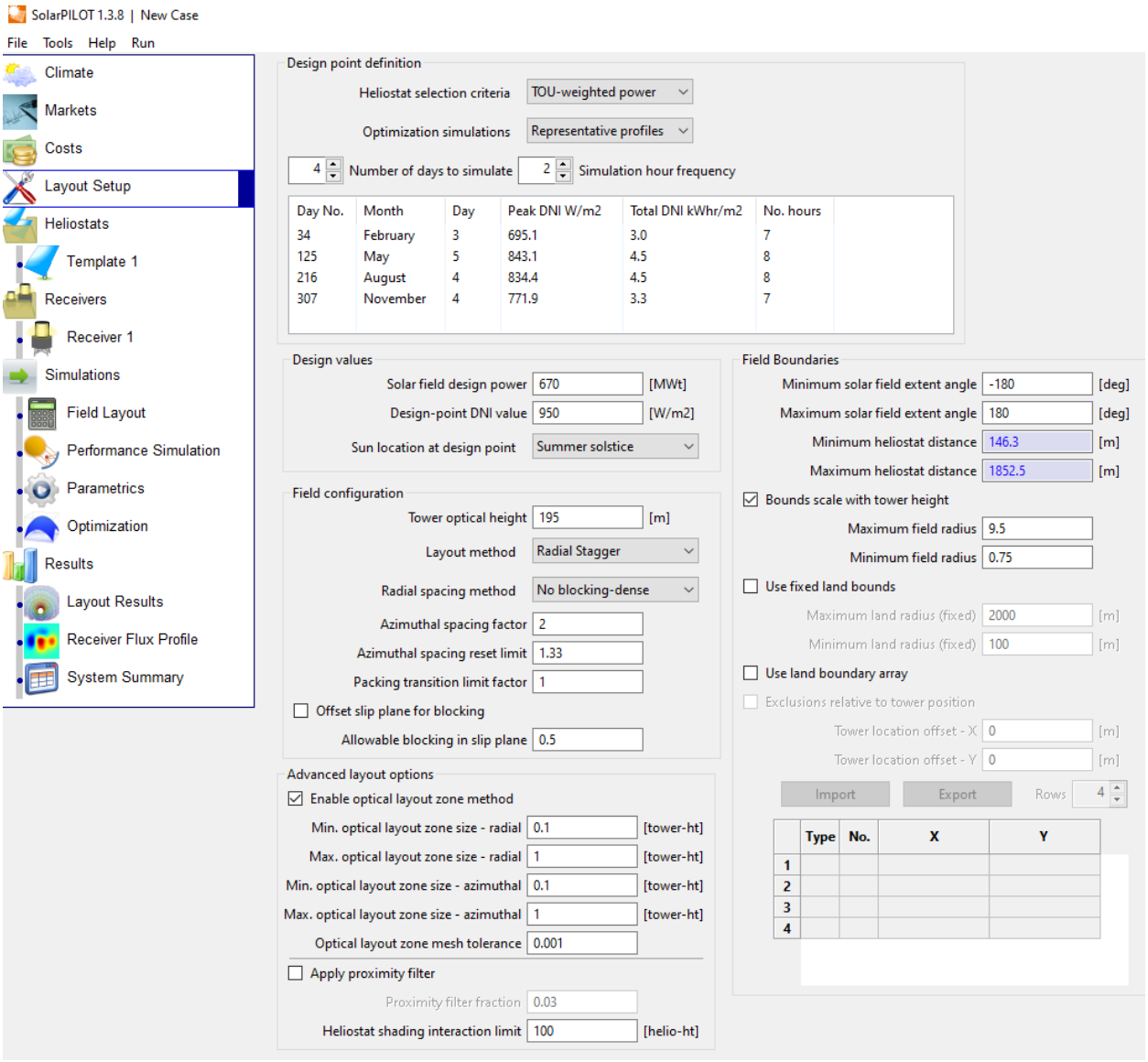

Figure 5. SolarPILOT Layout Setup. From this window, design parameters such as tower height, field boundaries as well as field configuration can be specified.

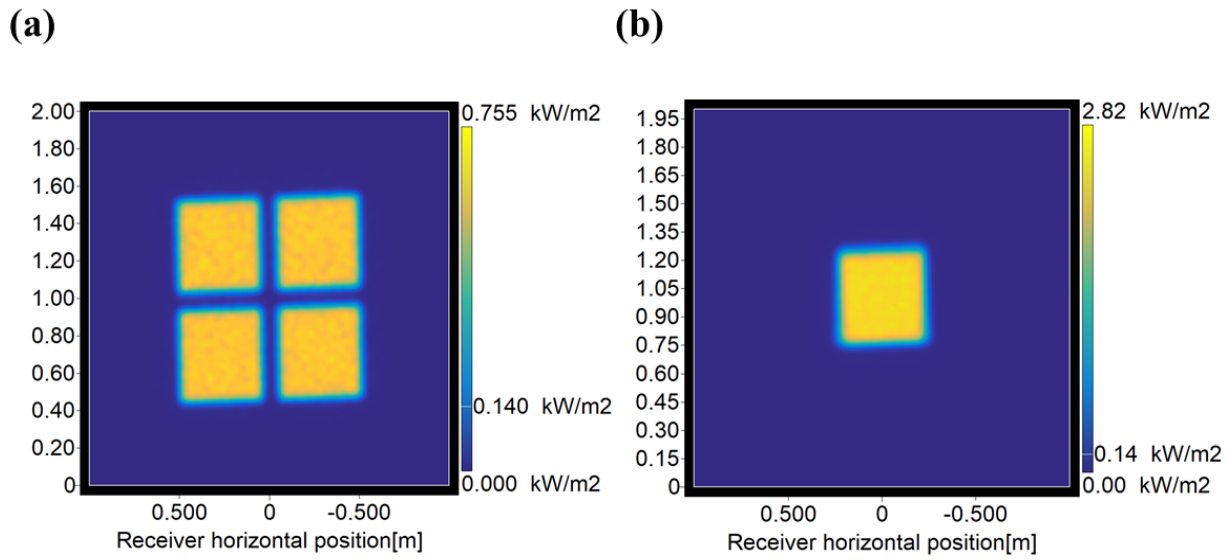

Figure 6. Flux distribution of canted heliostats (b) vs. non-canted heliostats (a).

3.1.3 Optical Efficiency

The optical efficiency η_{opt} of a heliostat field is the radiant power that enters the inlet aperture of the receiver divided by product of the total mirror area of the heliostats and the direct normal irradiance (DNI):

$$\eta_{\text{opt}} = \frac{Q_{\text{receiver}}}{\sum A_{\text{heliostat}} \cdot \text{DNI}} \tag{1.8}$$

Optical efficiencies presented in this chapter were automatically generated by SolarPILOT via simulation methods using SolTrace, a Monte-Carlo ray tracing engine.

3.1.4 Slope Error

Slope error θ_{err} is the angular difference between the measured surface normal and the ideal surface normal [20], defining how accurate a reflective surface is. Slope error, measured in milliradians, is a key contributor to optical efficiency in CSP towers as all heliostats are affected by it.

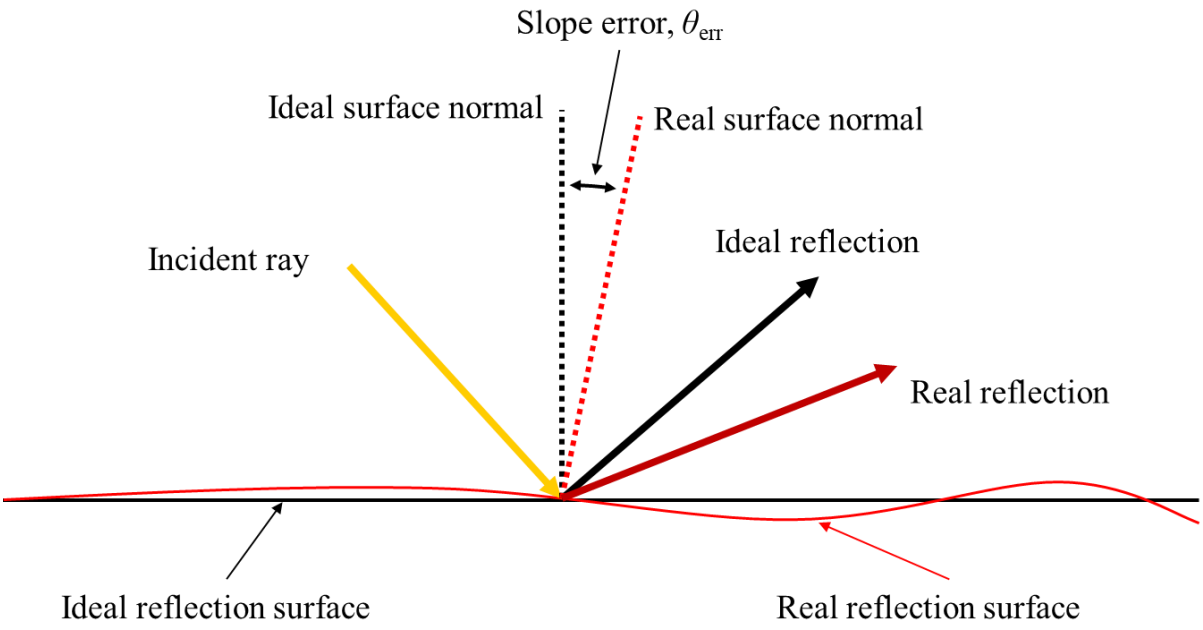

Figure 7. Visualization of slope error.

3.2 Results & Discussion

3.2.1 Multi Focus Field vs. 3 Single North Fields

Although heliostats are the most expensive component of solar tower systems, they can not be replaced as the number of heliostats determine the amount of solar radiation collected. However, there is no limitation to the number of cavity receivers that can be mounted on a single tower. Thus, the novel layout of mounting three receivers on a single tower, each with their own polar field of

heliostats, called a multi focus field, was proposed. The benefit of such a design reduces the number of towers needed for a system totaling three receivers as well as reduces the land area as all three polar fields point to a single tower, like a surrounding field.

To compare a multi focus field which has three receivers mounted on a single tower with three single receiver CSP towers, the goal was to first create a 1MW north facing power tower while being as optically efficient and economically efficient as possible. This meant that the aim was to have the tower height and receiver size to be as low and as small as possible, respectively. The key settings and parameters for such a field were the following: Tower height – 22m, Receiver size – 1.118m x 1.118m, Receiver Angle – negative 45°, Acceptance Angles - 90° horizontal / 70° vertical, Heliostats Size - 1m x 1m, Heliostat Panels - 2 x 2 (Canted with no gaps). To compare the single 1MW north facing power tower to a multi-focus 3 field tower, the design needed to be duplicated to have 3 separate north facing fields. The result is displayed in Figure 8 with the field converting at an average of 0.571 η_{opt}.

In order to compare and contrast the 3 north facing fields with a multi-focus design, the same design parameters were used in making the multi-focus field with the exception of specific land bounds. Although the horizontal acceptance angle was kept at 90°, 45° land bounds were put in place to ensure that there would be no heliostat interference between the north facing and east/west facing fields. The configuration is shown in Figure 9.

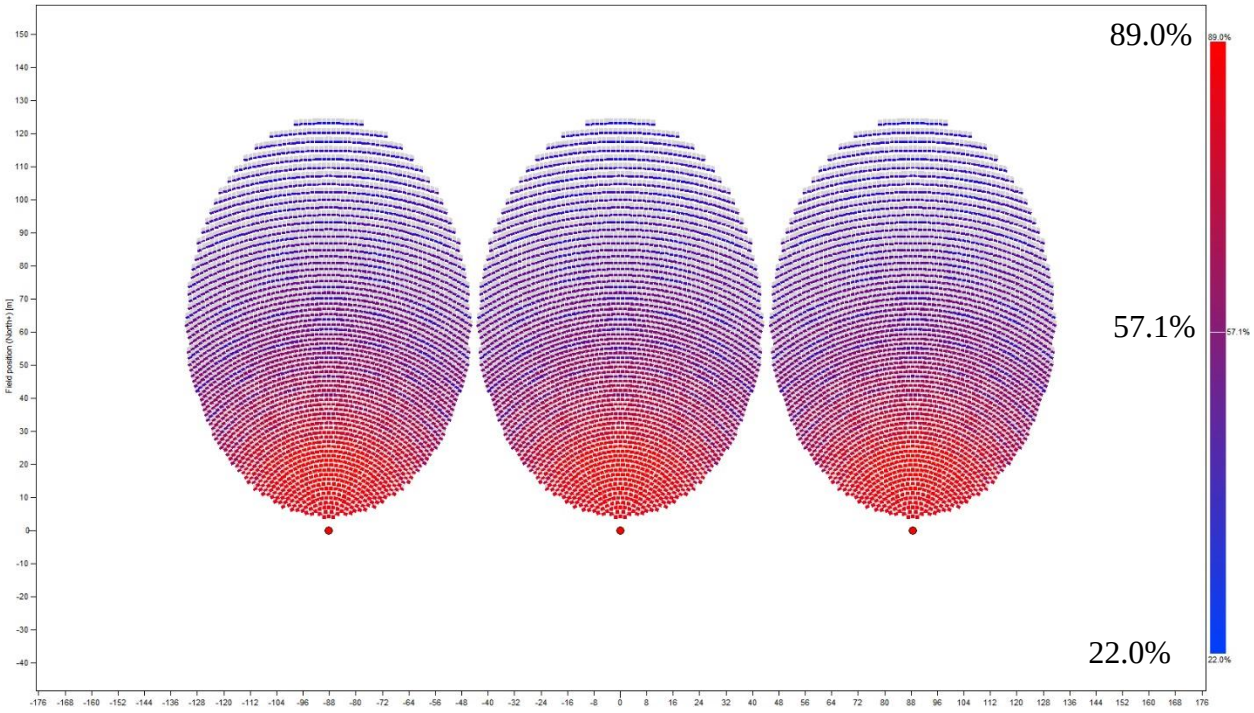

Figure 8. Three 1MW north facing power tower and field setups. The percentages on the right-hand side show the optical efficiency through coloured representation with the average being 57.1%.

56 parametric studies were conducted for both the single focus and multi-focus fields. The solar elevation and solar azimuth were both parameterized from 0°-70° and 90°-270°, respectively. The overall results showed that the changes in solar azimuth on average produced less than 5% relative standard deviation at the same solar elevation in terms of efficiency and power output. This suggests that the current norm of north facing fields has only a small advantage over other directions when the effect of the solar azimuth is small. Thus, all solar azimuths for the same solar elevation were grouped together for the results presented in this section. The number of heliostats in each field are as follows: multi-focus north (3074), multi-focus east and west (3191), and single north (3304). Figure 10 and Figure 11 show that although the single north field has the best overall performance, both the difference in efficiency and power to receiver are small and could be attributed to the higher number of heliostats. Figure 12 and Figure 13 present the comparison of

individual fields showing that the north field of the multi focus tower is similar to the single north field. It is important to note that the heliostats in closest proximity to the receiver are the best performing and carry the highest load in regard to overall efficiency as well as power. As shown in Figure 9, the 45° land bounds cut-off restricts many heliostats that could have otherwise been placed very close to the tower.

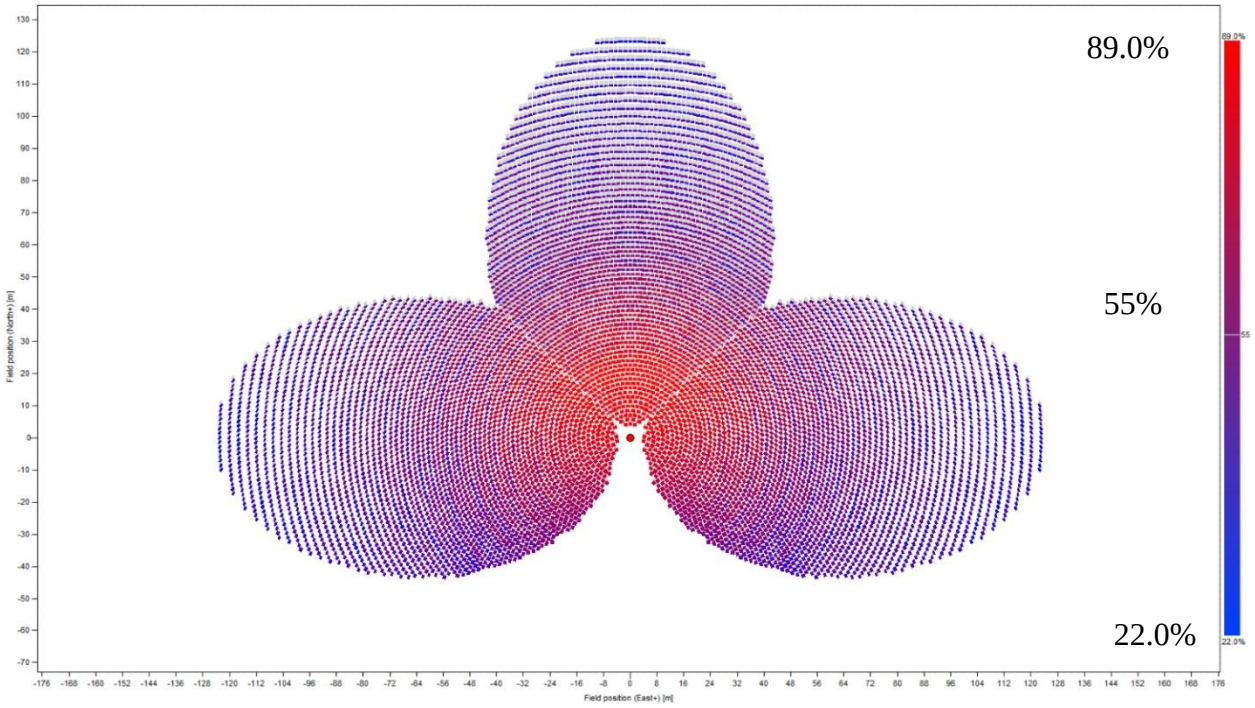

Figure 9. Multi-focus 1MW power tower and field setups. The percentages on the right-hand side show the optical efficiency through coloured representation with the average being 55%.

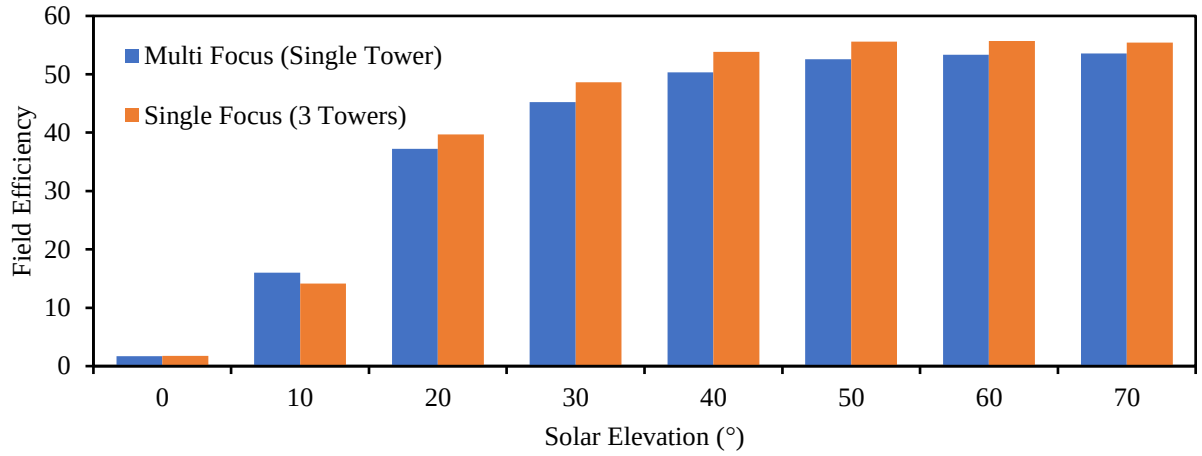

Figure 10. Optical efficiency vs. solar elevation comparison between multi focus single tower and single focus towers.

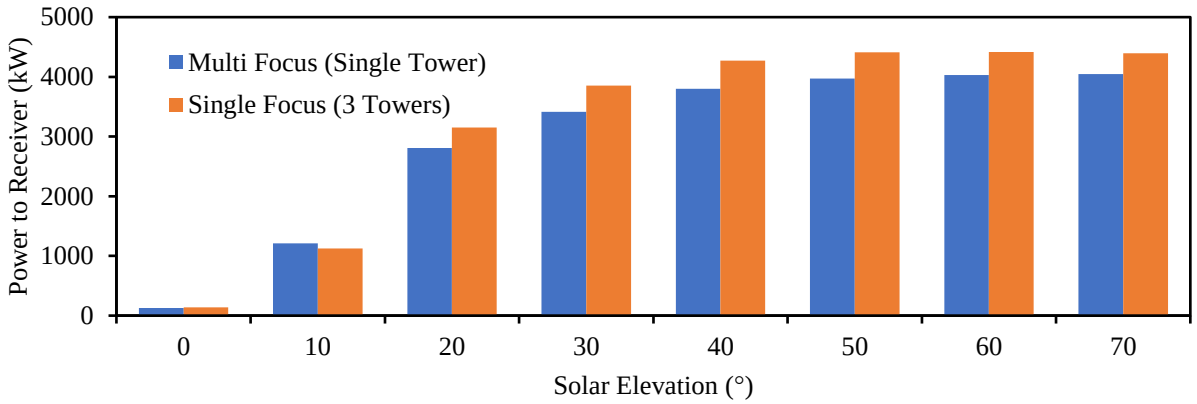

Figure 11. Power to receiver vs. solar elevation comparison between multi focus single tower and single focus towers.

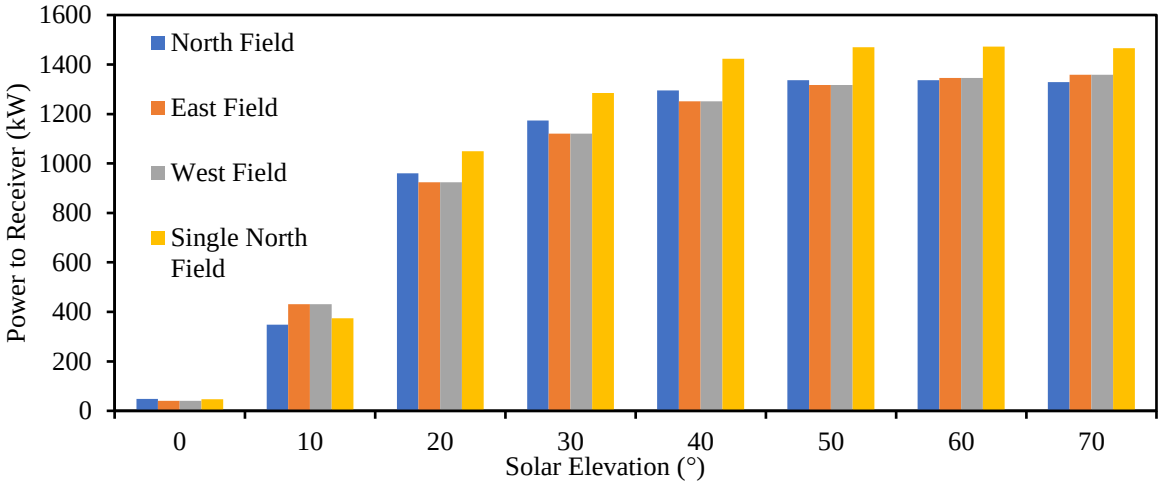

Figure 12. Power to receiver of individual fields vs. solar elevation.

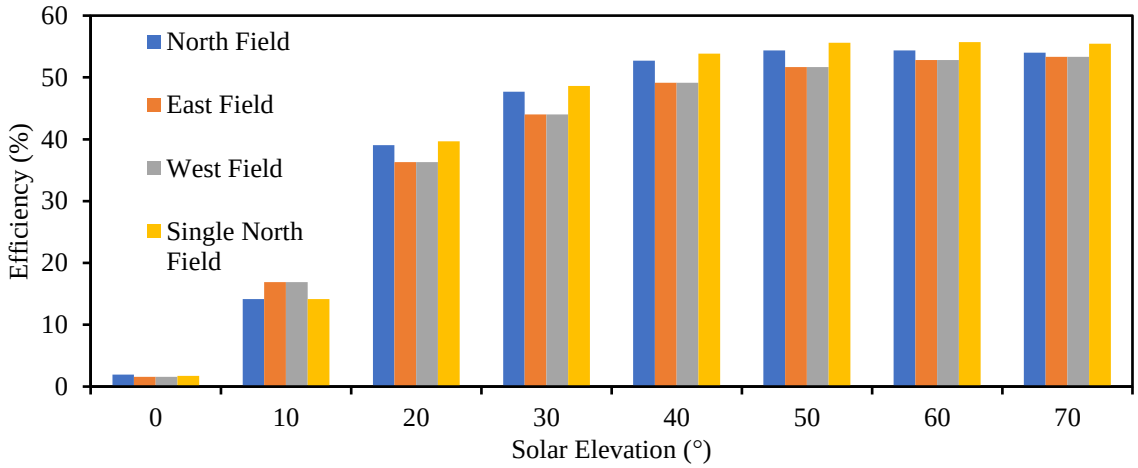

Figure 13. Optical efficiency of individual fields vs. solar elevation.

Upon further investigation, a very interesting trend regarding slope error appeared when comparing the north and east fields within the multi-focus tower system. Although the west field is not shown, it is expected to perform the same as the east field due to symmetry. In Figure 14 and Figure 15, 250 simulations were run for both the north and east fields with increasing slope

error and varying solar elevations and solar azimuths. The elevation and azimuths ranged from 0°-70° and 90°-270°, respectively. For the graphical representation, all azimuths and elevations were grouped together and evenly weighted, which includes some theoretical azimuth and elevation combinations that do not occur in real sun positions. Nevertheless, the east facing field showed that it was more resilient to slope error and outperformed the north facing field.

This is an unexpected result as the data indicates that north facing fields, despite being the norm, are not the best performing. However, this is very promising as the east and west fields seem to perform better when the slope error is increased. By association, the multi-focus tower performs better when the slope error is increased. Since slope error is an optical error, which often occurs in manufacturing of cheaper reflectors, this can be used to our advantage when designing for solar tower concentrators. Because heliostats are the most expensive component of concentrating solar tower plants, the potential to reduce the cost while maintaining power to receiver and relative efficiency levels makes multi-focus tower designs even more viable.

Based on the results presented in this chapter, a primary CSP tower cavity system can be designed to either be high in efficiency or be cheaper and capitalize on the use of a single tower with multiple fields. Nonetheless, both systems would benefit from the addition of a secondary concentrator which we hope to be both low cost and high performance. The design of such a secondary concentrator is discussed in the following chapter.

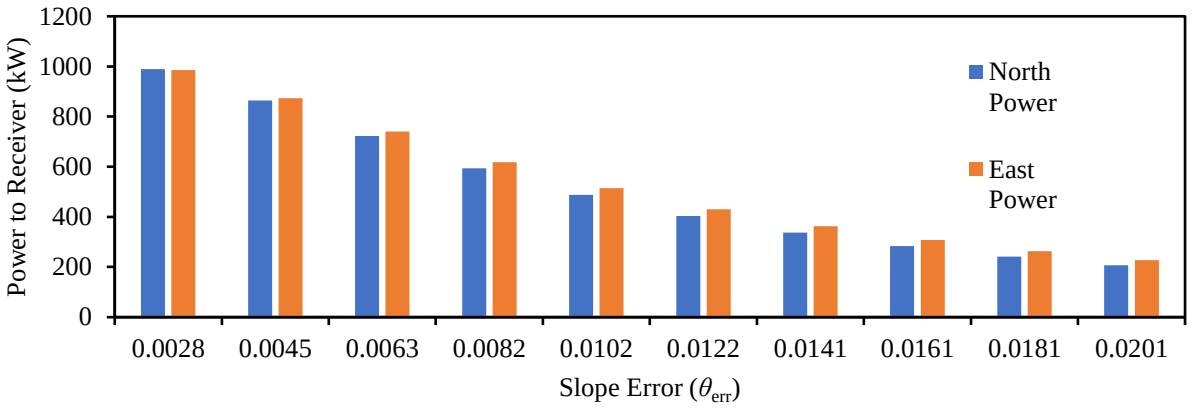

Figure 14. Power to receiver vs. slope error, in radians, comparison between the north and east fields within the multi focus tower.

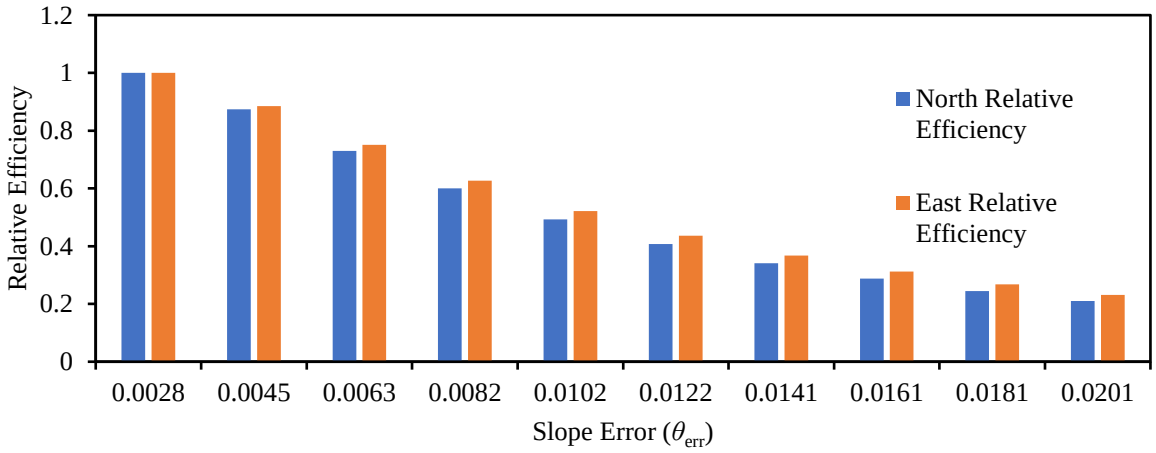

Figure 15. Relative efficiency vs. slope error, in radians, comparison between the north and east fields within the multi focus tower.

Chapter 4. Conical Secondary Concentrators

4.1 Geometric Definition

Compound parabolic concentrators, CPCs, are high performance secondary concentrators. Their role in CSP towers is to further concentrate the solar radiation that is reflected from the heliostat field toward the cavity receiver. The inlet of the CPC is the aim target for the heliostat field while the outlet of the CPC connects to the cavity receiver. The geometry of a CPC is fully defined by its outlet radius r_o and nominal acceptance half-angle θ_i. The concentration ratio and length of the CPC are given by Rabl and Winston [14], [15]:

$$C_g = \frac{A_i}{A_o} = \frac{\pi \cdot r_i^2}{\pi \cdot r_o^2} = \frac{1}{\sin^2 \theta_i} \tag{9}$$

and

$$l = \left(r_i + r_o\right) \cot \theta_i \tag{10}$$

The matched cone is a cone that spans directly from the inlet to the outlet circumferences of the underlying CPC as shown in Figure 16.

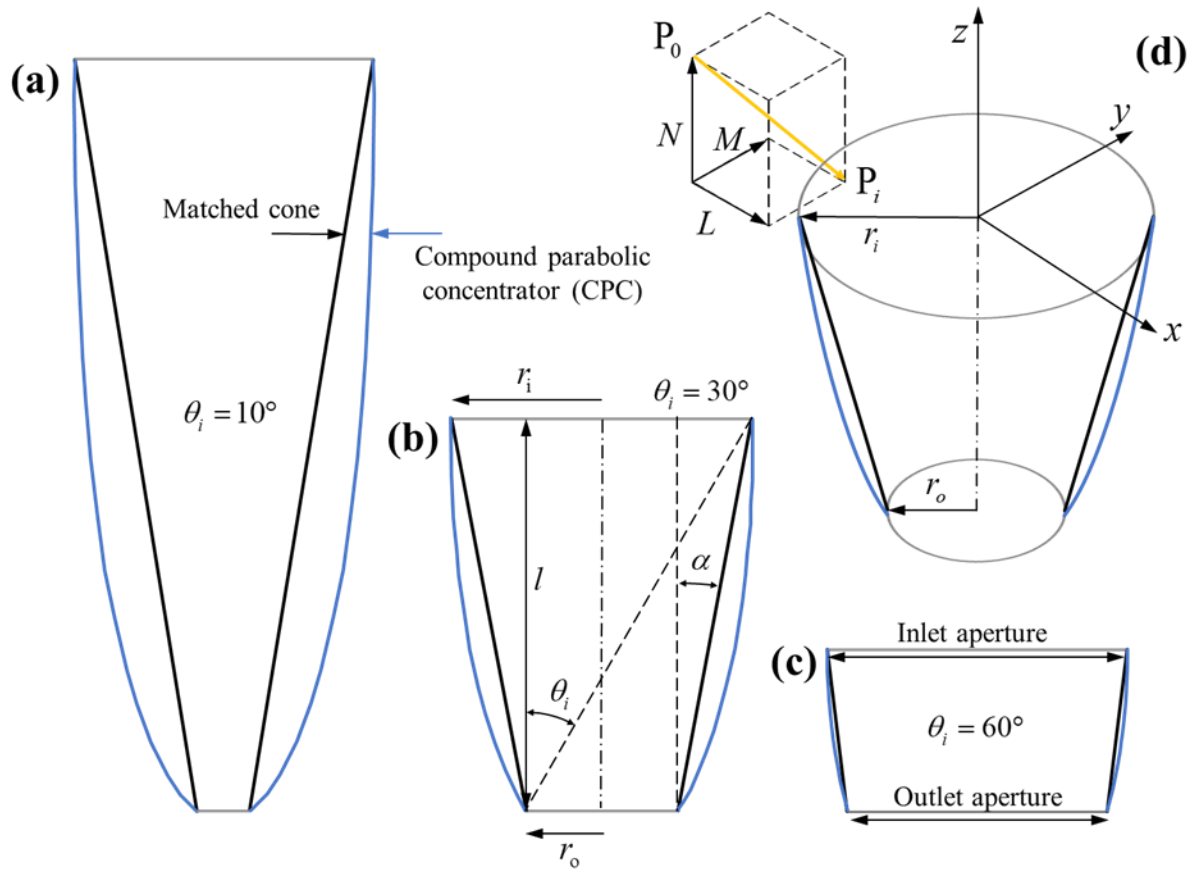

Figure 16. Coordinate system and geometry of various CPCs (blue) and matched cones (black). (a), (b) and (c) show θ_i = 10°, 30° and 60° geometries respectively. The way that the matched conical concentrator is designed is by connecting the same inlet and outlet circumferences as the underlying CPC. The result is a cone that has the same inlet and outlet apertures as well as length as the CPC. (d) depicts L, M and N direction-cosines of the unit vector, in the x, y and z directions, of a generic ray that originates at P_0 and enters the inlet at P_i. Acceptance angle θ_i, apex angle α, inlet radius r_i, outlet radius r_o and length l are visualized for the θ_i = 30° CPC & matched cone in (b).

The inlet and outlet apertures are connected by a simple side profile that is rotationally symmetric in the axial direction z. The apex angle α of the cone is measured between the side of the cone and the vertical axis and can be calculated using the following equation:

$$\alpha = \arctan\left(\frac{\tan\theta_i \cdot (1-\sin\theta_i)}{1+\sin\theta_i}\right) \qquad (11)$$

For all concentrator geometries in this thesis r_o is set at 1, including all matched cones and CPCs in Figure 16, without loss of generality since geometry and results can be accordingly scaled to any size.

The coordinate system of incoming rays and concentrators is depicted in Figure 16 (d). The definition of the unit direction vector follows similar conventions to Cooper et al. [18]:

$$\hat{\mathbf{v}} = \frac{\mathbf{P}_i - \mathbf{P}_0}{\left\|\mathbf{P}_i - \mathbf{P}_0\right\|} = \begin{bmatrix} L & M & N \end{bmatrix}^{\mathrm{T}} \tag{12}$$

$\mathbf{P}_0$ and $\mathbf{P}_i$ represent the origin of the ray and point at which the ray enters the geometry, respectively. *L*, *M*, and *N* are the direction-cosines in the *x*, *y*, and *z* directions. *L*, *M*, and *N* can each be calculated given the θ_{ray} in each direction through: $L = \cos\theta_{\text{ray, x}}$, $M = \cos\theta_{\text{ray, y}}$, $N = \cos\theta_{\text{ray, z}}$. *N* is seldom required in defining the ray since $L^2 + M^2 + N^2 = 1$ by definition of a unit vector and is taken to be negative by convention as the ray is travelling in the negative *z* direction towards the inlet aperture.

The relevant θ_i discussed in this paper span from 10°-60°. Interestingly for matched cones, the apex angle α remained relatively consistent ranging only between 7° and 11° as seen in Figure 17. This is a significant finding because one issue with the CPC is the inconvenience in its manufacturing. The cone is already easier to manufacture due to its straight side profile. The ability to constrict α to a small range while still matching the size and shape of various CPCs becomes another advantage of conical concentrators. The finding of matched cones' apex angles led to the investigation of fixing apex angles and is further discussed in this chapter.

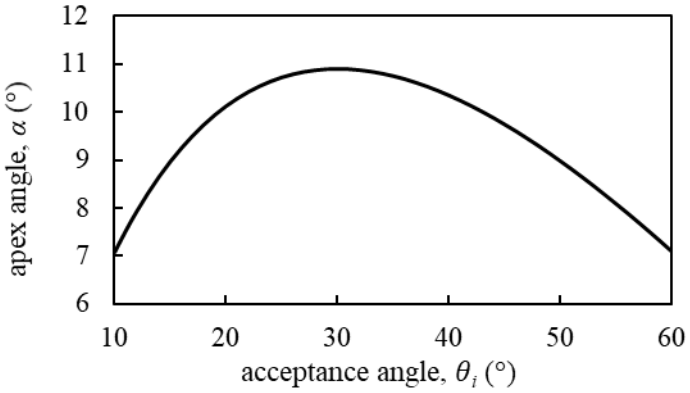

Figure 17. CPC acceptance angle vs. matched cone apex angle. All apex angles stay between 7° and 11° regardless of CPC size or C_g. For example, the 10° CPC (r_o = 1) has a length of 38.3 and C_g of 33.16 while the 60° CPC (r_o = 1) has a l of 1.24 and C_g of 1.33 yet both cones have very similar apex angles as seen in Figure 16 (a) and (c).

4.2 Performance Metrics

4.2.1 Acceptance & Optical Efficiency

Acceptance efficiency, η_{acc}, is a purely geometric property and describes the fraction of diffuse radiation that reach the exit aperture which enter through the inlet aperture and is not affected by optical properties such as reflectance ρ. The losses associated with η_{acc} are strictly caused by geometric rejection. Similarly, optical efficiency, η_{opt}, is affected by ρ and describes the ratio of the radiant power at the inlet aperture to the radiant power at the outlet aperture [21]. This can be expressed as the following:

$$\eta_{\text{opt}} = Q_o / Q_i \qquad (13)$$

where Q represents radiant power. When calculating for η_{opt}, surface reflectance ρ is considered as every interaction with the reflector's surface has the probability of absorption equal to $1-\rho$.

The losses associated with η_{opt} are caused by both geometric rejection as well as absorption. The method to calculate both η_{acc} and η_{opt} through MCRT simulations is the same and done by taking the fraction of radiation that reach the outlet aperture which carry Q_o divided by the fraction of rays which enter through the inlet aperture which carry Q_i. The distinction is that for acceptance efficiency, the reflectance of all mirror surfaces is set to 1.

4.2.2 Directional Acceptance

Directional acceptance η_{acc} is the acceptance efficiency when the source is collimated in a given direction with respect to the normal vector of the inlet aperture (the direction may be conveniently specified by *L* and *M* direction-cosines) with a uniform spatial distribution over the inlet aperture. Consequently, the acceptance value is then linked with those specific *L* and *M* direction-cosines. Since the geometries discussed in this paper are rotationally symmetric about the *z* axis, the directional acceptance is equal for all directions having equal θ_i, which can be expressed through the following: $\theta_i = \arcsin N = \arcsin\sqrt{L^2 + M^2}$. Equal θ_i means that $L^2 + M^2$ remains constant. When directional acceptance is displayed in two-dimensional space as a function of *L* and *M*, the resulting plot is referred to as the (directional) acceptance map of a concentrator. The purpose of creating an acceptance map is to show which directions are accepted and which are being rejected by the concentrator. Similarly, in one-dimensional representation, directional acceptance is displayed as a transmission-angle curve, $\eta_{acc}(\theta)$. This plot showcases concentrators' acceptance behavior as incoming radiation angle θ_{ray} is increased from 0 to angles above θ_i as shown in Figure 19.

4.2.3 Average Number of Reflections

The average number of reflections, $\langle n_r \rangle$, is self-explaining in that it describes the average number of reflections that an accepted ray undergoes as it travels from the inlet of the concentrator to the outlet. $\langle n_r \rangle$ is also a purely geometric quantity meaning that it is not affected by surface properties such as ρ. The significance of investigating $\langle n_r \rangle$ is that the effects on η_{opt} are compounded when the $\langle n_r \rangle$, ρ, and l of a geometry are all taken into consideration.

4.3 Results & Discussion

4.3.1 Acceptance & Optical Efficiency

To investigate optical efficiency η_{opt}, 51 CPCs and corresponding matched cones were constructed at each θ_i between 10° and 60°. Their inlet apertures were evenly illuminated with diffuse radiation with a max $\theta_{\text{ray}} = \theta_i$. Figure 18 shows the direct comparison of η_{opt} between the CPC and its matched cone. From Figure 18, we see that the difference in performance between both of the $\rho = 1$ and $\rho = 0.9$ cases decreased as the acceptance angle, θ_i increased from 10° to 60°. This can be attributed to both the CPC and matched cone geometries. As the θ_i increases, these following two entities see a decrease: C_g and l. Both of which are conducive in allowing for the direct entry of incoming rays to reach the outlet aperture. The nearly converging shape between the matched cone curves at ρ = 1 and ρ = 0.9 suggest that the effect of absorptance is less prominent at smaller l. Moreover, the decreased C_g results in a more cylindrical like cone with lower cone angle α as the difference in r_i and r_o decreases resulting in lower geometric rejection. Similarly, infinitely

long cones, with perfect reflectance, have no geometric rejection and have perfect acceptance efficiency [22]. The effects of C_g and l are further discussed in Chapter 4.3.4.

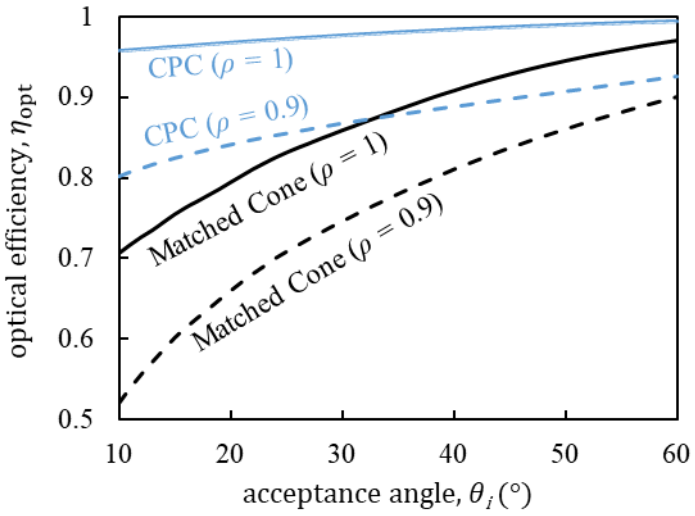

Figure 18. Optical efficiency of CPC vs. matched cone. The difference in shape profiles between the ρ = 1 and ρ = 0.9 cases is a direct result of absorptance and the rays' interactions with the reflector surface. In the ρ = 1 simulation, the optical efficiency is the same as its acceptance efficiency and can be considered a purely geometric property as there's no absorptance. Any rays that are rejected in the ρ = 1 simulations are rejected due to the receiver geometry. 10^7 rays were traced per simulation.

4.3.2 Transmission-angle Curves

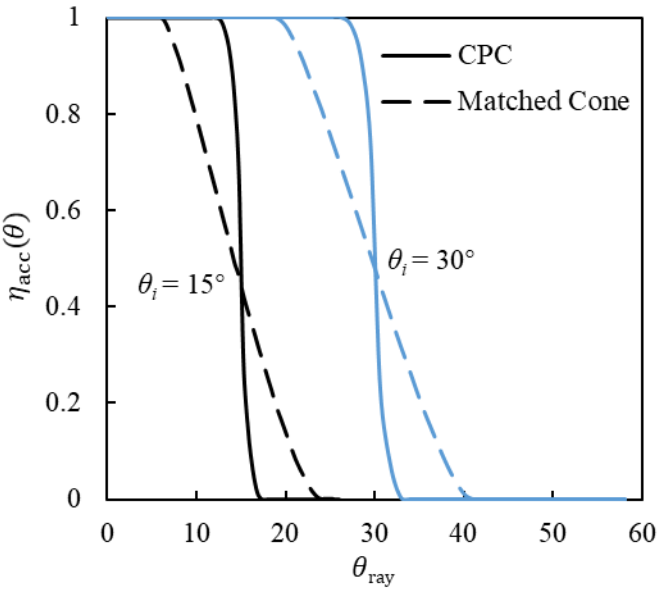

Figure 19. Transmission-angle curves for CPCs and matched cones for θ_i = 15° and θ_i = 30°. 10^5 rays were traced in each simulation.

Transmission-angle $\eta_{acc}(\theta)$ curves depict a geometry's ability to accept an incoming ray based on the direction θ_{ray} that the ray enters the concentrator [23]. The transmission-angle curves in Figure 19 show the circumferential average of the directional acceptance map, as seen in Figure 20, of two geometries at two different θ_i, 15° and 30°. Furthermore, since the directional acceptance maps are axisymmetric, it is also a radial slice through the map in any direction. The CPC appears to be the best at accepting rays within its θ_i while rejecting all rays above it. In theory, an ideal light collector will accept all incoming rays entering its aperture with incident angles less than its θ_i and reject all rays with angles greater (i.e. a step function transmission-angle curve). However, real concentrators show that the cutoff occurs through a range of over 1°, centered about θ_i, regardless of what that θ_i is [24]. Simulation results in Figure 19 demonstrate that the cutoff occurs over a range of 4° for the 15° CPC and 6° for the 30° CPC which supports Gleckman's claim that

transmission-angle curves appear rounded near θ_i due to skew ray losses [23]. Meanwhile, the matched cone performed poorly in comparison showing ray rejection well below θ_i but showing acceptance behavior above it. While acceptance outside of θ_i may be advantageous in specific cases, Collares-Pereira et al. noted that any radiation gained from outside the designated θ_i comes at a loss of radiation from inside the θ_i [25]. This finding is plausible seeing that even though the matched cone appears to make up for its ray rejection within θ_i with acceptance above it, the overall η_{acc} is still unable to rival that of the CPC.

4.3.3 Directional Acceptance Efficiency

Directional acceptance η_{acc} is the directional dependent acceptance efficiency when evenly distributed, collimated rays enter the inlet aperture. The significance of this property is that it allows for the determination of which angles are geometrically accepted and which are geometrically rejected. To investigate directional acceptance, the incoming ray direction needed to be represented by a range of L and M direction-cosines. The relevant L, M space of the concentrator was sampled using a 101 by 101 grid of individual L, M points. The 10201 points of η_{acc} were then used to create an acceptance map, as seen in Figure 20 which shows the directional dependent performance of the matched cone and CPC at $\theta_i = 15°$, $\theta_i = 30°$, $\theta_i = 45°$, and $\theta_i = 60°$. The concentrators are axisymmetric meaning their directional acceptance maps should show the same symmetry as is observed in Figure 20. A circle of radius sin θ_i which represents the acceptance map of an ideal concentrator, is superimposed as a dashed red line. An overall trend in the performance of both sets of concentrators is that rejection within θ_i decreases as θ_i increases. The CPC appears to have the best ability to accept within θ_i while rejecting all rays outside it. The

matched cone is able to provide comparable directional acceptance to the CPC at $\theta_i = 45°$ and $\theta_i = 60°$ but demonstrates significant rejection within θ_i at $\theta_i = 15°$ and $\theta_i = 30°$.

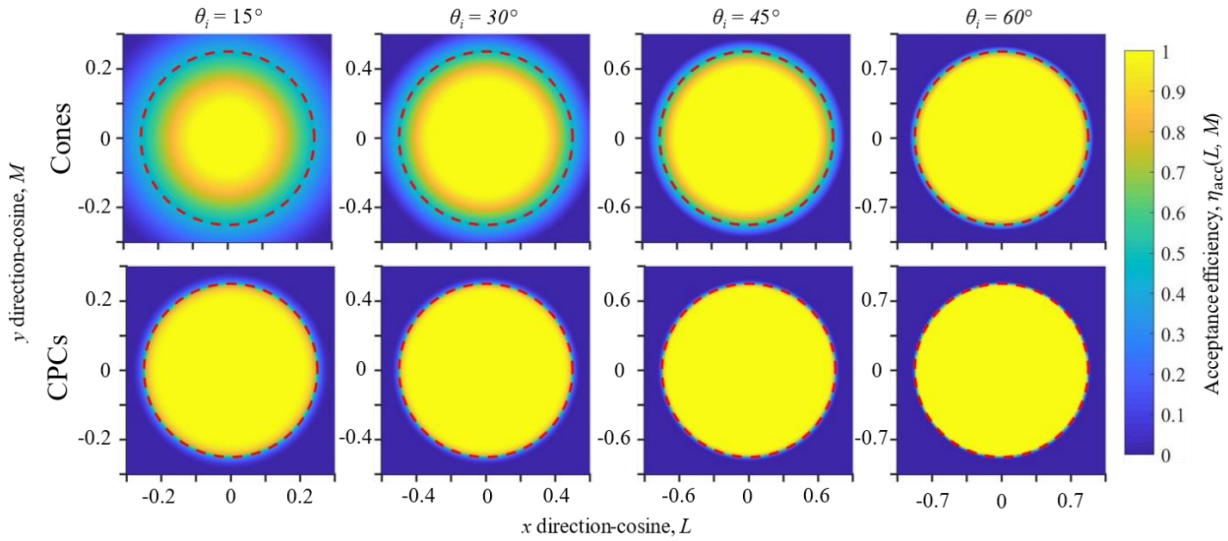

Figure 20. Directional acceptance for matched cones (top row) and CPCs (bottom row). The red dashed circle on each plot has a radius of sin θ_i, which is the designed acceptance radius of an ideal concentrator. 10^5 rays were traced per grid point (101 by 101 grid) totaling 10^9 rays per plot.

4.3.4 Cone Angle and Cone Length

The motivation behind this investigation stemmed from the relatively constant apex angles α of the matched cones as θ_i ranges from 10°-60° from Figure 17. The main advantage of keeping α fixed is that it could potentially make the conical concentrator simple to manufacture in that a single die could be used to form concentrators of all C_g. The cones in Figure 21 (a) were constructed by first referencing the matched cone. The l between the inlet and outlet is then adjusted to match the desired α. Similarly, the cones shown in Figure 21 (b) were constructed by taking the matched cone and multiplying the l by a factor while keeping C_g constant. The results suggested that lower α resulted in higher η_{acc}. However, upon further investigation, it was found that the lower α cones only performed better because of their longer lengths as demonstrated by

the 2, 5, and 10 *l* cones in Figure 21 (b). The evidence shown in the figure proves that *l* rather than α is the determinant in a cone's performance.

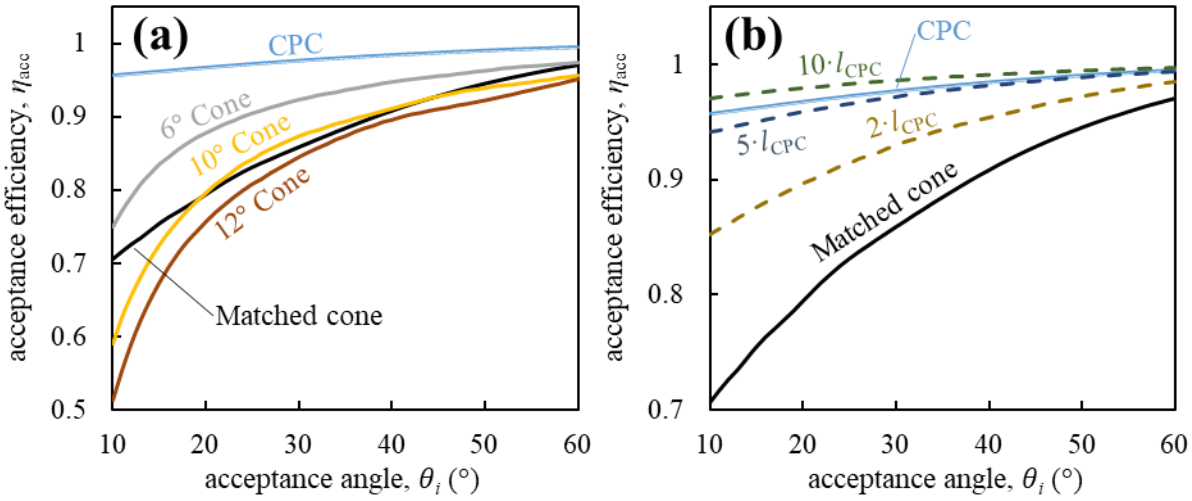

Figure 21. Acceptance efficiency as a function of acceptance angle for (a) cones having a fixed apex angle and (b) cones having a length as a multiple of the underlying CPC. The acceptance efficiency for the underlying CPC is also shown for comparison. All simulations shown in this figure were run using $\rho = 1$. The inlet and outlet apertures remained consistent with their CPC counterparts meaning that for all designs at a given acceptance angle, the C_g was the same. For (a), cones are longer or shorter than the CPC depending on the choice of apex angle compared to that of the matched cone c.f. Figure 17. For (b), the apex is chosen to achieve the desired length multiple vis-a-vis the matched cone. 10^7 rays were traced per simulation.

The 10° cone was one of particular significance because its performance was very close to that of the matched cone. Thus, a more detailed exploration of the 10° cone was conducted and the results are plotted in Figure 22. When $\rho = 1$, the 10° cone outperforms the matched cone between θ_i of 20°-42° which is attributed to the 10° cone's longer length at this range. When $\rho = 0.9$, the performance of the two cones were nearly identical throughout. The extra cone length needed for the 10° can be justified by the constant α and ability to use a single die.

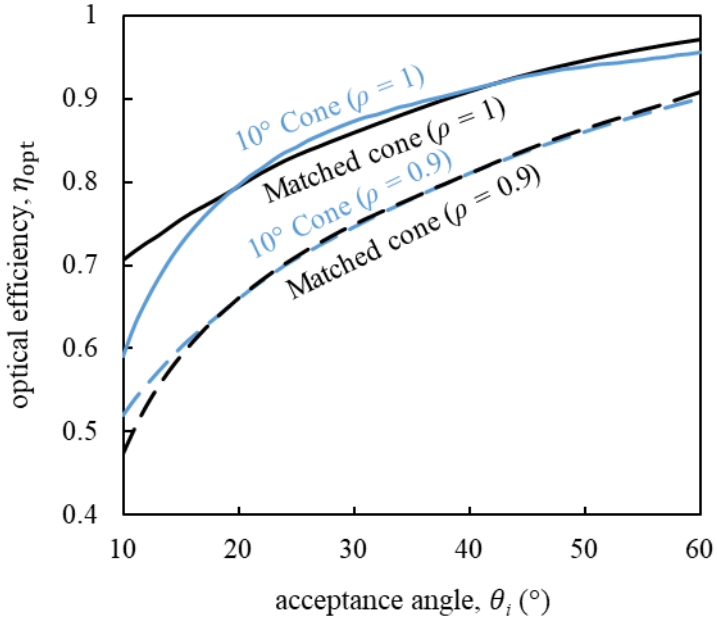

Figure 22. Fixed 10° cone vs. matched cone optical efficiency comparison. The comparison at both ρ = 1 and ρ = 0.9 indicate that the 10° cone is a viable substitute for the matched cone. 10^8 rays were traced per simulation.

The previous results earlier in this section indicated that l is the determining factor on performance, so this a closer look was taken to verify that claim. For each CPC θ_i: 10°, 30°, and 60°, the fixed C_g cone is sized to the inlet and outlet aperture of the corresponding CPC which also has a length ratio l_{cone}/l_{CPC} of 1. This set the reference size and the inlet and outlet radii remained fixed. The only variable was l, which also resulted in the change in α for every cone. For a purely geometric and academic study, the reflectance was set to 1 and l_{cone}/l_{CPC} between 1 and 20 were simulated where the diffuse ray source was kept to the same as the θ_i of the reference CPC. 500 simulations were conducted per θ_i. This verified Welford and Winston's claim that infinitely long cones with perfect reflectance are have 100% acceptance as shown in Figure 23 [22]. The cones were able to match ρ = 1 CPC performance at 5-7 l_{cone}/l_{CPC} ratios. Meanwhile, a cone with a length multiple of 10 always outperforms a CPC in terms of η_{acc}, for θ_i:10°-60°, as depicted by Figure 22. From a

more practical standpoint, ρ was set to 0.9 to explore the effects of combining perfect acceptance by geometry with realistic absorption. The study was conducted in the exact same way except l_{cone} / l_{CPC} ranged between 0.1 to 5. η_{opt} initially increased with l, but eventually peaked and began to decrease as seen in Figure 23 (b). This is due to the increased number of reflections and the effect of absorption from $\rho = 0.9$. These cones were never able to match the ρ = 0.9 CPC performance and peak η_{opt} ranged from 0.6-1.2 l_{cone}/l_{CPC}. Hahm identified the practical dilemma of choosing between energy lost through absorption and energy lost through geometric rejection [26]. A cone of infinite length provides maximum acceptance but suffers from a high number of reflections. Meanwhile, a cone of very short length minimizes the average number of reflections but suffers from geometric rejection.

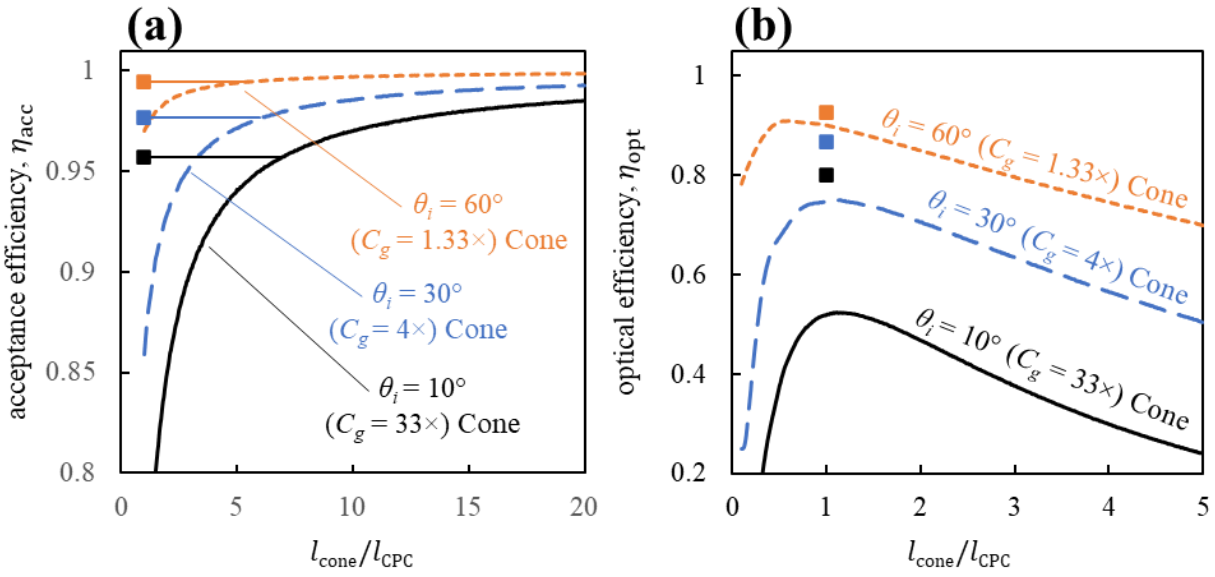

Figure 23. Optical efficiency of fixed C_g cones as a function of the ratio between cone length and CPC length at ρ = 1 (a) and ρ = 0.9 (b). The performance of each respective CPC is marked by the square on the graph at x = 1. In (a), the intersection between the CPC marker and cone acceptance efficiency corresponds to the length of the cone required to match the acceptance efficiency of the CPC, which occurs at x coordinates of l_{cone}/l_{CPC} = 5.4-7. In (b), the ρ = 0.9 cones performed best between l_{cone}/l_{CPC} = 0.6-1.2, but the optical efficiency of the CPC is never matched at any cone length. 10^6 rays were traced per simulation.

4.3.5 Average Number of Reflections

The average number of reflections $\langle n_r \rangle$ is an important aspect of concentrator design. To investigate the effect that $\langle n_r \rangle$ has on a concentrator, this study was conducted to verify the claim that higher number of reflections causes lower efficiency [27] while at the same time aiming to validate equations by Rabl & Cooper et al.. Rabl had presented the following equation as an approximation of optical efficiency based off of acceptance efficiency, reflectivity and average number of reflections [28], [29]:

$$\eta_{\text{opt}} = \eta_{\text{acc}} \cdot \left\langle \rho^{n_r} \right\rangle \approx \eta_{\text{acc}} \rho^{\langle n_r \rangle} \tag{14}$$

Meanwhile, a convenient solution to calculate for $\langle n_r \rangle$ was presented by Cooper at al. [18]:

$$\langle n_r \rangle \approx \frac{1}{\eta_{\text{acc}}} \frac{\eta_{\text{acc}} - \eta_{\text{opt}}\big|_{\rho=1-\Delta\rho}}{\Delta\rho} \tag{15}$$

The error associated with Eq. (15) is equal to the order of $\Delta\rho$ and Eq. (15) can only be considered as exact in the limit as $\Delta\rho$ approaches 0 [18]. A reasonable choice for $\Delta\rho$ is 0.01 for which Eq. (15) becomes the following:

$$\langle n_r \rangle = \frac{1}{\eta_{opt}|_{\rho=1}} \frac{\eta_{opt}|_{\rho=1} - \eta_{opt}|_{\rho=0.99}}{0.01} \tag{16}$$

The choice to use 0.01 for $\Delta\rho$ is to ensure that the difference between $\eta_{\text{opt}}|_{\rho=1}$ and $\eta_{\text{opt}}|_{\rho=0.99}$ is greater than their combined MCRT error, or noise floor. Considering the numerator in Eq. (16), there will be two MCRT error terms, one from each simulation of $\eta_{\text{opt}}|_{\rho=1}$ and $\eta_{\text{opt}}|_{\rho=0.99}$. Therefore,

as $\Delta\rho$ approaches 0, the difference between $\eta_{opt}|_{\rho=1}$ and $\eta_{opt}|_{\rho=1-\Delta\rho}$ approaches 0 as well. However, the two MCRT error terms remain, causing $\langle n_r \rangle$ to become an invalid answer. In a similar secondary concentrator simulation, Cooper et al. demonstrated that simulations with 10^8 rays traced are expected to have random MCRT error lying within the range of 10^{-3} and 10^{-4} [18]. To verify that Eq. (14) is a reasonable approximation, the predicted η_{opt} values needed to be compared with MCRT simulation values. η_{acc} is a required prerequisite in Eq. (14) while the $\langle n_r \rangle$ was calculated using Eq. (15). If the differences between the MCRT values and the predicted values are small, then Eq. (14) can determine the η_{opt} of a shape for any ρ that we know $\langle n_r \rangle$ and η_{acc}.

MCRT simulations were run for CPCs, matched cones and 10° cones between θ_i = 10°-60° at both ρ = 1 and ρ = 0.99 for η_{opt}. These two values of η_{opt} were used in Eq. (16) to calculate for $\langle n_r \rangle$ and plotted in Figure 24. The values of $\langle n_r \rangle$ and $\eta_{opt}|_{\rho=1}$, or η_{acc}, were then used in Eq. (14) to predict η_{opt} at ρ = 0.9. The predicted η_{opt} for CPCs and matched cones of ρ = 0.9 were plotted and compared to MCRT simulated values of η_{opt}. The results are displayed in Figure 25 showing very little difference across all θ_i suggesting that Eq. (14) would prove to be valid at other ρ values as well.

Regarding Figure 24, the CPC has fewer reflections than both cones below θ_i =49°, while the matched cone has fewer reflections than the 10° cone between the range of θ_i =19- 41°. Interestingly, the 10° cone outperforms the matched cone between θ_i =20- 42° when $\rho = 1$ as seen in Figure 22. This suggests that the increased acceptance efficiency from the increased length outweighs the additional reflection losses. This anomaly further solidifies the 10° cone as a viable substitute to the CPC.

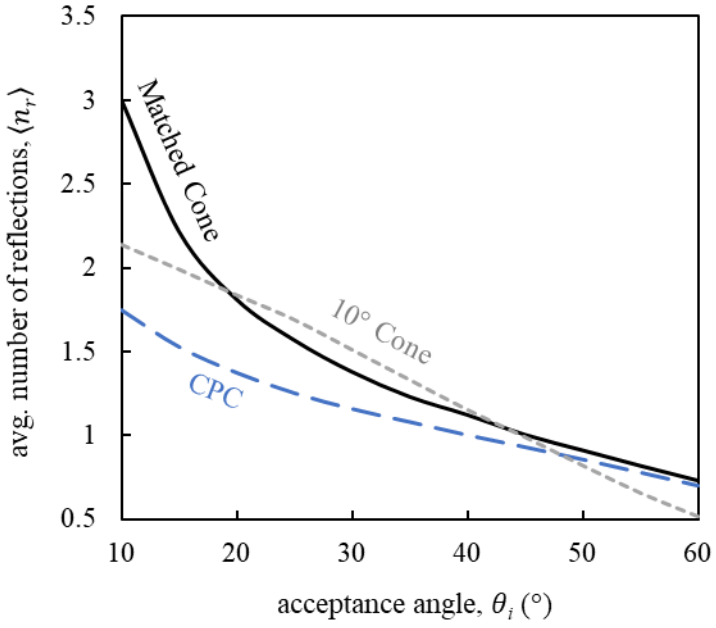

Figure 24. Average number of reflections. 10^8 rays were traced per simulation.

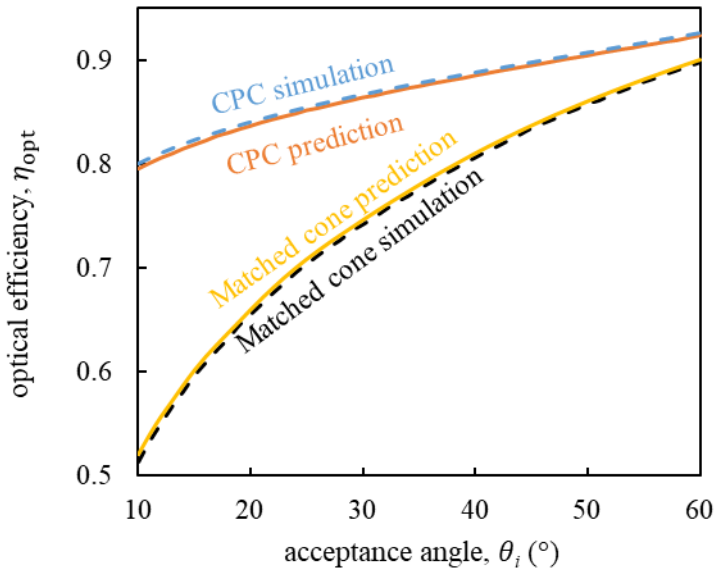

Figure 25. Comparison of simulated optical efficiency vs. optical efficiency predicted using Eq. (14) at ρ = 0.9. The agreement between the curves indicate that Eq. (14) does a good job of predicting the combined effect of ray rejection and ray absorption. 10^8 rays were traced per simulation.

4.3.6 A Design Map for Conical Concentrators

When designing a conical concentrator, the two key design parameters are concentration ratio and length. C_g dictates the θ_i and therefore should be appropriately selected based on the incoming source. However, higher C_g often results in lower optical efficiency as the cone's apex angle α increases, causing greater geometric rejection as shown in Figure 26.

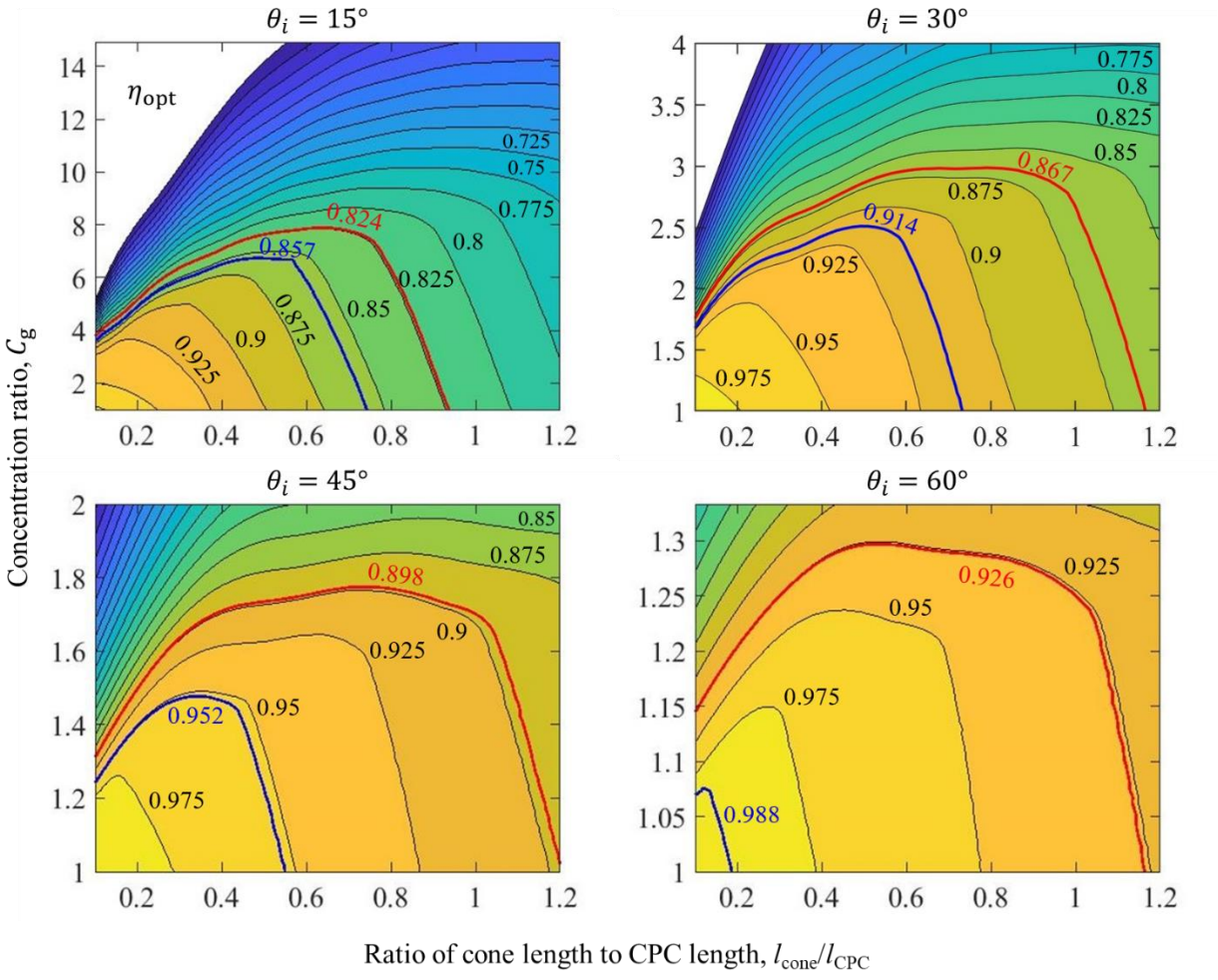

Figure 26. Conical concentrator design map. The red line represents the performance of the θ_i CPC while the blue line represents the performance of the same θ_i CPC truncated to 81% of its C_g. This design map can be utilized to construct cones to meet design specifications in η_{opt}, C_g or l. 10^7 rays were traced per simulation.

Similarly, the length of the cone affects η_{opt} as well. As l decreases, the cone's α increases given that C_g remains constant meaning that more geometric rejection occurs. As l increases for cones with imperfect reflective surfaces, absorption increases due to the increased number of average reflections. Therefore, it would be extremely beneficial for optical designers to have a cone design map that allowed them to either match the CPC in either C_g or η_{opt}.

The map was designed to investigate the effect of manipulating the C_g and l to find optimal cone designs for various CPC θ_i and other requirements. All simulations presented in Figure 26 used ρ = 0.9 as it is a common design value used for secondary concentrators. The plot will indeed change for different ρ values, but it is expected that the ρ = 0.9 plot is suitable and sufficient for most practical applications. In a 1980 study, Myer illustrated the relationship between cone inlet, outlet and length required to accept paraxial rays based off Williamson's findings in 1952 [30][31]. This can be used as a guideline after the concentration ratio has been picked to determine if the length picked for the cone will accept or reject paraxial rays. According to Myer, a cone to match a 30° CPC should have the following dimensions: If r_o = 1 and r_i = 2 then the length should be at least 1.732 (approximately 0.33 l_{cone}/l_{CPC}). The four plots in Figure 26 show the effects of adjusting C_g and l_{cone} about the size of the θ_i CPC. The cone C_g ranges from 0.25-1 CPC C_g through the adjustment of r_i while the l_{cone} ranges from 0.1-1.2 l_{CPC} over 60 steps. Cones were designed to achieve the same η_{opt} as the CPC and is represented all along the red lines while the η_{opt} of the truncated CPCs are marked in the blue lines. Due to the shape of CPCs near their inlet aperture, a large portion can be truncated without much sacrifice in C_g. Therefore, truncated CPCs can provide high C_g at lower l and reflector surface area. The idea of reducing reflector area without sacrificing any concentration is discussed by Baum where 2D ideal compound parabolic wedge concentrators

were manipulated such that the sides were shortened from the receiver end to reduce surface area [32]. η_{opt} is presented as contour plots with 0.025 between each line. Evidently, the region that shows the highest η_{opt} is at the bottom left corner where the cone is the shortest in length while having the lowest C_g. Ideally, the highest performing cones would be at the upper left corner where C_g is the greatest and l_{cone} is smallest. However, the best realistic option would be to choose a cone in the left region of where the red (CPC) curve begins to plateau. This way, the same η_{opt} of the CPC or greater can be achieved while keeping the l_{cone}/l_{CPC} as low as possible but comes at a cost of lower C_g. Nonetheless, the plots can be used to prioritize other cone characteristics or design specifications as well.

4.3.7 Conical Concentrator for Solar Towers

The conical concentrator design map in Figure 26 was put to the test to pair a conical concentrator with a solar tower system. The goal was to investigate the effect on overall system efficiency, as defined in Equation (1.17), that a conical secondary concentrator would have on a SPT system. An assumption for cavity temperature was made to be 1500 °C, or 1773.15 K.

The single tower north field described in Chapter 3.2.1 has the following specifications: Receiver size – 1.118 m^2, Acceptance Angles - 90° horizontal / 70° vertical. Therefore, a conical receiver with an inlet diameter of 1.118 m and θ_i = 45° is chosen to accommodate for the maximum width of the receiver and the maximum horizontal acceptance angle, respectively.

One caveat from the SolarPILOT simulations from Chapter 3.2.1 is that they were run with a square receiver. This means that only radiation within a circle inscribed the 1.118 m^2 square

receiver can enter the inlet aperture of a conical concentrator. Figure 27 shows the circular flux profile at the following design parameters: DNI = 800 W/m^2, Solar azimuth = 180°, and Solar elevation = 40°. Since radiation outside of the inscribed circle does not enter the secondary concentrator's inlet, the radiation is considered lost. This means that the system's optical efficiency needs to be multiplied by an image intercept factor of 0.9362 to account for the new effective receiver area. The image intercept factor is calculated by normalizing the original square flux data from SolarPILOT and determining which points are inside the circle to compare the flux sum between what is on the inside and what is on the entire receiver. With 3074 heliostats in the single north field each measuring 1 m^2, they provide a primary C_g of 3131.34.

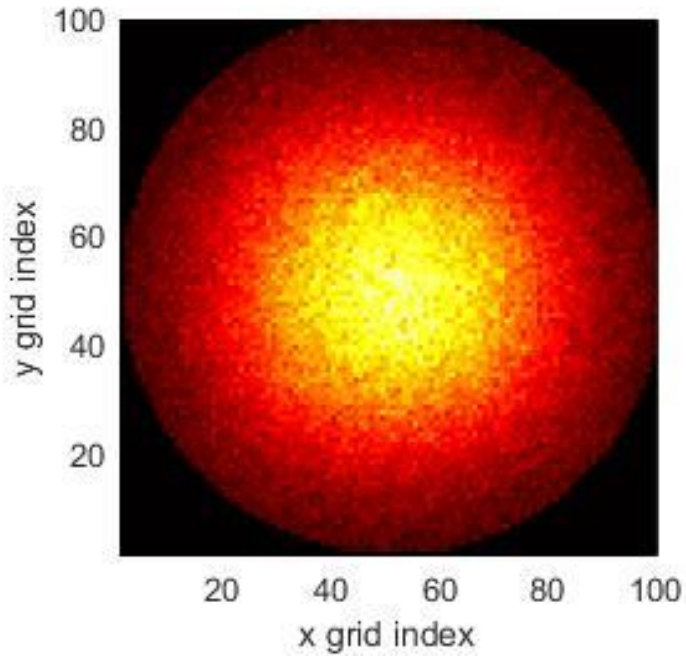

Figure 27. Circular aperture receiver flux profile of a single north solar tower.

For this application, the θ_i = 45° design map from Figure 26 is used to design a conical concentrator. The goal was to meet the efficiency of the CPC (0.898) while keeping C_g as high as possible. η_{opt}

= 0.8985 was achieved when the l_{cone}/l_{CPC} was 0.6 and C_g was 1.75. Overall dimensions of the conical secondary concentrator are as follows: r_i = 0.559 m, r_o = 0.423 m, l = 0.572 m. This conical secondary concentrator would provide an additional C_g of 1.75 at 0.8985 η_{opt}. The overall C_g with the conical secondary concentrator is then 5479.85. Given that the average efficiency of the single north field system was 57.1%, the new average efficiency would be 48.0%, when paired with this secondary, and factoring in the image intercept factor and the η_{opt} of the cone.

To compare overall system efficiency between the SPT with and without the conical secondary concentrator, Equation. (1.17) is used.

$$\text{Eff} = 1 - \frac{\sigma T^4}{q} \tag{1.17}$$

where σ is the Stefan-Boltzmann constant ($5.67 \cdot 10^{-8}$ $W \cdot m^2 \cdot K^{-4}$), T is temperature in Kelvin (1773.15 K), and q is the product of optical efficiency, concentration ratio, and DNI.

$$q = \eta_{opt} \cdot C_g \cdot \text{DNI} \tag{1.18}$$

The overall system efficiency without the secondary is then 58.15% and 73.38% with a conical secondary concentrator. As a result, the addition of a single conical secondary concentrator is able to boost the C_g from 3131.34 to 5479.85 as well as increase the overall efficiency of the SPT system by 15.23%.

Chapter 5. Conclusions and Outlook

5.1 General Conclusions

The viability of a multi focus CSP tower configuration with a single tower was investigated via SolarPILOT. The simulation results have shown that the multi-focus tower setup is viable as the efficiency and power to receiver levels are competitive with the single north facing towers while using less heliostats and with two fewer towers and a smaller land requirement. The advantage that the east and west fields have over the north facing field when slope error is increased indicates perhaps that the norm of north facing solar towers are not necessary for optimal configuration. The advantages of the side fields have when the slope error is increased can be utilized to make more cost-effective solar tower concentrators because the most expensive component of CSP towers are the heliostats.

Cones are considered as secondary concentrators to boost the concentration from the primary solar tower configuration. The size difference between the inlet and outlet apertures of cones results in additional flux concentration conductive for ultra-high temperature cavity receivers. The optical performance of cones and conical approximations to the CPC were investigated via MCRT methods. As θ_i increased from 10°-60°, the difference in η_{opt} between the cone and CPC decreased. Although the cone showed geometric rejection at direction-cosines lower than the designed sin θ_i, it did demonstrate some levels of directional acceptance above sin θ_i. For all θ_i: 10°-60°, the α of the matched cone remained between 7°-12°. Most interestingly, a fixed 10° performed nearly identically to the matched cone at $\rho = 0.9$ while providing higher η_{acc} at $\rho = 1$. It was also verified that l was the most significant design metric when $\rho = 1$ as infinitely long cones proved to be

perfect concentrators with η_{acc} approaching 1. The effect of $\langle n_r \rangle$ was investigated while validating equations from Rabl and Cooper et al. which grants the ability to predict η_{opt} for any ρ when η_{acc} and $\langle n_r \rangle$ are known. A design map is then presented with varying C_g and l_{cone} values to allow the design for conical concentrators of any η_{opt} with arbitrary C_g and l_{cone}. Evidently, the η_{opt} was highest when both C_g and l_{cone} were at their lowest because of low geometric rejection and lower absorptance. However, the recommended cone design at each θ_i would be to choose a cone with $l_{cone} < l_{CPC}$ at a lower C_g to maintain η_{opt}. The cone and conical approximations proved to be viable substitutes to the CPC with advantages such as consistent α across all θ_i as well as ease of manufacturing. Thus, the conical concentrator has the potential to fulfil many optical concentration requirements.

5.2 Outlook

Future studies to build upon the work described in this thesis may include:

- Annual simulations to investigate CSP tower performance for specific locations with their respective weather files to determine the compatibility of the CSP system and location.
- Conduct complete ray tracing models that originate from source to heliostat, which is reflected to the secondary concentrator, and finally the receiver. Ray tracing simulations have been run for both the CSP tower and secondary concentrator, but they have been done individually. Combining the two would provide additional accuracy as the rays entering

the secondary concentrator would be directionally dependent on the heliostat field as opposed to being evenly and randomly distributed.

- Pair the conical secondary concentrator design with existing CSP systems based off their acceptance angles and field configurations. This would further validate the versatility of conical concentrators and their ability to be designed to any concentration ratio and optical performance specifications.

The proposed single focus solar tower designs can be used as references for solar towers of various sizes and power requirements. Meanwhile, the parameters of conical secondary concentrators can be adjusted to accommodate for length and concentration ratio while remaining cost effective. Ultimately, this work sets the stage for improved solar tower design for ultra-high temperature solar receiver applications.

Chapter 6. References

[1] P. Breeze, *Power generation technologies*, 3rd ed. 2019.

[2] M. Whitaker, G. Heath, P. O'Donoughue, and M. Corum, "Life Cycle Greenhouse Gas Emissions of Coal Fired Electricity Generation: Systematic Review and Harmonization," *J. Ind. Ecol.*, vol. 16, no. 1, pp. 53–72, 2012, [Online]. Available: http://www.nrel.gov/docs/fy13osti/56487.pdf.

[3] B. Belgasim, Y. Aldali, M. J. R. Abdunnabi, G. Hashem, and K. Hossin, "The potential of concentrating solar power (CSP) for electricity generation in Libya," *Renew. Sustain. Energy Rev.*, vol. 90, no. March, pp. 1–15, 2018, doi: 10.1016/j.rser.2018.03.045.

[4] NREL, "Concentrating Solar Power Projects," 2022. https://solarpaces.nrel.gov/by-technology/power-tower.

[5] X. Xu, K. Vignarooban, B. Xu, K. Hsu, and A. M. Kannan, "Prospects and problems of concentrating solar power technologies for power generation in the desert regions," *Renew. Sustain. Energy Rev.*, vol. 53, pp. 1106–1131, 2016, doi: 10.1016/j.rser.2015.09.015.

[6] M. T. Islam, N. Huda, A. B. Abdullah, and R. Saidur, "A comprehensive review of state-of-the-art concentrating solar power (CSP) technologies: Current status and research trends," *Renew. Sustain. Energy Rev.*, vol. 91, no. November 2017, pp. 987–1018, 2018, doi: 10.1016/j.rser.2018.04.097.

[7] A. A. Rizvi, S. N. Danish, A. El-Leathy, H. Al-Ansary, and D. Yang, "A review and classification of layouts and optimization techniques used in design of heliostat fields in solar central receiver systems," *Sol. Energy*, vol. 218, no. October 2020, pp. 296–311, 2021, doi: 10.1016/j.solener.2021.02.011.

[8] O. Behar, A. Khellaf, and K. Mohammedi, "A review of studies on central receiver solar thermal power plants," *Renew. Sustain. Energy Rev.*, vol. 23, pp. 12–39, 2013, doi: 10.1016/j.rser.2013.02.017.

[9] X. Wei, Z. Lu, Z. Lin, H. Zhang, and Z. Ni, "Optimization procedure for design of heliostat field layout of a 1MWe solar tower thermal power plant," *Solid State Light. Sol. Energy Technol.*, vol. 6841, no. January 2008, p. 684119, 2007, doi: 10.1117/12.755285.

[10] Y. Zhang, Y. Qiu, Q. Li, and A. Henry, "Optical-thermal-mechanical characteristics of an ultra-high-temperature graphite receiver designed for concentrating solar power," *Appl. Energy*, vol. 307, no. July 2021, p. 118228, 2022, doi: 10.1016/j.apenergy.2021.118228.

[11] H. Yang, Y. Xu, A. Acosta-Iborra, and D. Santana, "Solar tower enhanced natural draft dry cooling tower," *AIP Conf. Proc.*, vol. 1850, no. June, 2017, doi: 10.1063/1.4984393.

[12] R. P. Merchán, M. J. Santos, A. Medina, and A. Calvo Hernández, "High temperature central tower plants for concentrated solar power: 2021 overview," *Renew. Sustain. Energy Rev.*, vol. 155, p. 111828, 2021, doi: 10.1016/j.rser.2021.111828.

[13] A. Steinfeld and A. Meier, "Thermochemical Production of Fuels with Concentrated Solar

Energy," *5th FORUM NEW Mater. PART C*, vol. 74, no. April, pp. 303–312, 2010, doi: 10.4028/www.scientific.net/ast.74.303.

[14] A. Rabl, "Comparison of solar concentrators," *Sol. Energy*, vol. 18, no. 2, pp. 93–111, 1976, doi: 10.1016/0038-092X(76)90043-8.

[15] R. Winston, "Cone collectors for finite sources," *Appl. Opt.*, vol. 17, no. 5, pp. 688–689, 1978, [Online]. Available: https://doi.org/10.1364/AO.17.000688.

[16] M. J. Wagner and T. Wendelin, "SolarPILOT: A power tower solar field layout and characterization tool," *Sol. Energy*, vol. 171, no. August 2016, pp. 185–196, 2018, doi: 10.1016/j.solener.2018.06.063.

[17] J. Petrasch, "A Free and open source monte carlo ray tracing program for concentrating solar energy research," pp. 1–8, 2010.

[18] T. Cooper, F. Dähler, G. Ambrosetti, A. Pedretti, and A. Steinfeld, "Performance of compound parabolic concentrators with polygonal apertures," *Sol. Energy*, vol. 95, pp. 308–318, 2013, doi: 10.1016/j.solener.2013.06.023.

[19] K. R. Bhargav, F. Gross, and P. Schramek, "Life cycle cost optimized heliostat size for power towers," *Energy Procedia*, vol. 49, pp. 40–49, 2014, doi: 10.1016/j.egypro.2014.03.005.

[20] J. K. Stynes and B. Ihas, "Slope error measurement tool for solar parabolic trough collectors," *World Renew. Energy Forum, WREF 2012, Incl. World Renew. Energy Congr. XII Color. Renew. Energy Soc. Annu. Conf.*, vol. 2, no. April, pp. 948–955, 2012.

[21] D. G. Burkhard, G. L. Strobel, and D. L. Shealy, "Solar concentrating properties of truncated hexagonal, pyramidal and circular cones," *Appl. Opt.*, vol. 17, no. 15, p. 2431, 1978, doi: 10.1364/ao.17.002431.

[22] W. T. Welford and R. Winston, *High Collection Nonimaging Optics*. London: Academic Press, 1989.

[23] P. Gleckman, "Achievement of ultrahigh solar concentration with potential for efficient laser pumping," *Appl. Opt.*, vol. 27, no. 21, p. 4385, 1988, doi: 10.1364/ao.27.004385.

[24] R. Winston, "Light Collection within the Gramework of Geometrical Optics," *J. Opt. Soc. Am.*, vol. 60, no. 2, pp. 245–247, 1970.

[25] M. Collares-Pereira, J. O'Gallagher, and A. Rabl, "Approximations to the CPC-a comment on recent papers by Canning and by Shapiro," *Sol. Energy*, vol. 21, no. 3, pp. 245–246, 1978, doi: 10.1016/0038-092X(78)90028-2.

[26] T. Hahm, H. Schmidt-Traub, and B. Leßmann, "A cone concentrator for high-temperature solar cavity-receivers," *Sol. Energy*, vol. 65, no. 1, pp. 33–41, 1999, doi: 10.1016/S0038-092X(98)00119-4.

[27] H. Schmidt-Kloiber and H. Schoeffmann, "Metallic hollow cones as light concentrators," *Appl. Opt.*, vol. 25, no. 2, p. 252, 1986, doi: 10.1364/ao.25.000252.

[28] A. Rabl, "Optical and thermal properties of compound parabolic concentrators," *Sol. Energy*,

vol. 18, no. 6, pp. 497–511, 1976, doi: 10.1016/0038-092X(76)90069-4.

[29] A. Rabl, “Radiation transfer through specular passages-a simple approximation,” *Int. J. Heat Mass Transf.*, vol. 20, no. 4, pp. 323–330, 1977, doi: 10.1016/0017-9310(77)90153-3.

[30] J. H. Myer, “Collimated radiation in conical light guides,” *Appl. Opt.*, vol. 19, no. 18, p. 3121, 1980, doi: 10.1364/ao.19.003121.

[31] D. E. Williamson, “Cone Channel Condenser Optics,” *J. Opt. Soc. Am.*, vol. 42, no. 1949, pp. 712–715, 1952.

[32] H. P. Baum and J. M. Gordon, “Optimal design of nonimaging solar concentrators with wedge receivers,” *Appl. Opt.*, vol. 24, no. 16, pp. 2596–2599, 1985, [Online]. Available: https://doi.org/10.1364/AO.24.002596.